A nonlinear piezoelectric shunt absorber with a 2:1 internal resonance: Theory

Zein A. Shami [a,*], Christophe Giraud-Audine [b], Olivier Thomas [a]

[a] Arts et Metiers Institute of Technology, LISPEN, HESAM Université, F-59000 Lille, France
[b] Arts et Metiers Institute of Technology, L2EP, HESAM Université, University Lille, Centrale Lille, HEI, F-59000 Lille, France

A B S T R A C T

In this paper, a semi-passive nonlinear piezoelectric shunt absorber is presented, aiming at attenuating the vibration of a resonant elastic structure under external excitation. This is done by connecting the elastic structure to a nonlinear shunt circuit via a piezoelectric patch. The nonlinear shunt circuit consists of resonant circuit that includes a quadratic non-linearity. A particular tuning of the natural frequency of the shunt enables to create a two to one internal resonance. This generates a strong coupling between the mechanical mode and the electrical mode, leading to replace the mechanical resonance with a nonlinear antiresonance associated with an amplitude saturation, thus leading to an efficient vibration reduction. In this paper, we first propose a theoretical model that is expanded onto a suitable electromechanical modal basis and reduced to the two modes of interest, nonlinearly coupled by quadratic terms. Then, analytical solutions are obtained by the multiple scale method and compared to a reference numerical solutions stemming from the harmonic balance method. This enables to investigate the performance of the system in term of vibration absorption as well as giving design rules to tune the nonlinear shunt and to choose the free parameters of the system.

1. Introduction

Vibration reduction is an important research field in many engineering applications, especially in the industrial machine design and in the sectors where lightweight structures can be used. One of the efficient strategies that took a wide range of interest the past 20 years is the electrical shunt damping family of techniques, due to its efficient vibration attenuation properties and to its ease of set and control. It consists in using an electromechanical transducer to convert the vibratory energy of the host structure into electrical energy in a dedicated electronic circuit, designed to dissipate it and/or to counteract the structure's vibrations. Depending on the physics of the transducer, piezoelectric or electromagnetic, shunts have been proposed in the pioneering works [1,2] and have been addressed in a huge number of contribution since (see [3,4] and reference therein). Contrary to active control for which independent sensors and actuator are connected in closed loop, the shunt principle consists in using a single transducer, that serves as sensor and actuator at the same time when connected to a suitable electronic circuit. In most shunt architectures, the system is unconditionally stable, contrary to active control strategies.

A large majority of shunts are linear, the simplest architecture being the electromechanical analogs of mechanical dynamical dampers such as Frahm (also called dynamic vibration absorber, DVA) or Lanchester dampers [5,6], also called respectively resonant and resistive shunts [7]. In the case of a piezoelectric transducer, equivalent to a capacitor C, the resonant shunt consists in using a

* Corresponding author.
E-mail addresses: zein_alabidin.shami@ensam.eu (Z.A. Shami), christophe.giraud-audine@ensam.eu (C. Giraud-Audine), olivier.thomas@ensam.eu (O. Thomas).

simple inductor L as electronic circuit (and eventually an additional resistor R) to obtain a resonant RC (RLC) circuit coupled to a given mode of the primary mechanical structure [7,8]. More complex architectures can include a negative impedance to improve the performances [9] or be based on periodic piezoelectric transducers architectures for multimode damping [10].

However, it might be interesting to benefit from special dynamical phenomenon related to nonlinearities, examples of which are given in the recent reviews [11,12]. In the field of nonlinear absorbers, several families of strategies have been proposed in the past, firstly using mechanical devices and then being sometimes transposed to electromechanical analogs. The first family of absorbers, currently known as "nonlinear energy sinks" (NES) and using the so-called principle of "targeted energy transfer", was originally proposed in 2001 [13]. In the original concept, it consisted in attaching to a primary linear structure an essentially nonlinear oscillator into which the vibratory energy is transferred and localized. Because of the essentially nonlinear properties of the absorber, its free oscillation frequency strongly depends on the amplitude of the motion and there is always an amplitude for which the two oscillators lock in frequency, leading to an irreversible energy transfer (precisely through a one to one internal resonance). Since then, a huge amount of works emerged (more than one hundred selected publication are mentioned in the recent review [14]). We cite here some of them, relevant to us because they explain the design rules and propose several types of nonlinearities: [15] for cubic spring smooth stiffness, [16] for polynomial magnetic stiffness, [17] for a bistable stiffness and [18] for vibro-impact nonlinearities. The extension of the mechanical NES to piezoelectric devices has been theoretically proposed in [19] and recently realized, for the first time, with an analog circuitry (using multipliers) in [20]. It was also recently proposed in [21] in an active control philosophy, using force feedback.

A second family is the one of the so-called "nonlinear tuned vibration absorbers" (NLTVA), introduced in [22], that are a generalization of the classical DVA adapted for primary structures which have nonlinearities. Indeed, those nonlinearities, in most cases, lead to a dependence of the characteristic frequencies (free oscillations, resonance, antiresonance…) upon the amplitude of the motion. Consequently, a DVA, which has to be tuned to a particular fixed frequency, will correctly work on a limited range of amplitude. In contrary, the NLTVA is designed to present nonlinearities similar to those of the primary system. It is then naturally able to adapt itself to the dynamics of the primary structure for a large amplitude range. Since the pioneering work [22], the principle has been investigated in several studies using mechanical absorbers (see [23] and reference therein). The extension of NLTVA to piezoelectric shunts has been theoretically proposed in [24] and experimentally demonstrated in [25] with passive only electronic components and in [26] with a digital signal processor connected to the piezoelectric patches by analog electronic interfaces made of operational amplifiers.

The third family of nonlinear absorbers is composed of the synchronized switch damping (SSD) strategies. They consist in switching the electromechanical transducer on two distinct shunt impedances, synchronously with the oscillations of the host structure. This idea was initially proposed in [27,28] for piezoelectric transduction and developed in numerous contributions since then (see [29] for a recent review). Those SSD techniques are adaptive, intrinsically stable, require low power but their effect can be viewed as a resonance peak reduction, proportional to the excitation amplitude, similarly to traditional resistive or resonant shunts, with higher performance for one degree of freedom host structure [30].

The fourth family of nonlinear absorbers is based on the use of internal resonances. In a nonlinear system, if the ratio of two modal frequencies ω_i and ω_j is a rational number, namely $q\omega_i \simeq p\omega_j$ with $p, q \in \mathbb{N}^*$, a strong coupling between the two corresponding modes can occur, leading to particular exchanges of energy between the modes. This is called a p:q internal resonance and (ω_i, ω_j) can be the (linear) natural frequencies of the modes as well as there nonlinear extension (the frequencies of the nonlinear modes, that depend on the amplitude of the motion). On the first case, the internal resonance is observed at low amplitude and is often a consequence of a particular geometry, obtained with symmetries (1:1 internal resonance are encountered in beams/strings of symmetric cross section [31], in circular/square plates [32,33], in cylindrical shells [34] and spherical caps [35]) or by intentional tuning, in musical instruments (1:2, 1:2:4 and 1:2:2:4:4:8 internal resonances are encountered in gongs and steel-pans [36,37]) or in micro-systems applications [38–40]. In the second case of an internal resonance with the nonlinear free oscillation frequencies, the coupling appear at larger amplitude, when the change of frequencies due to the amplitude of the motion is compatible with the frequency relationship (see e.g. [41,42]).

When two modes of a system with quadratic nonlinearities fulfills a 1:2 internal resonance ($\omega_2 \simeq 2\omega_1$), the modal coupling leads to energy exchanges that occur at different frequencies (if the energy is injected to the second mode resonance near ω_2, it is transferred to the first mode at half the driving frequency. On the contrary if the first mode is resonantly driven near ω_1, the energy is transferred to the second mode at twice the driving frequency, near $\omega_2 \simeq 2\omega_1$. To signify the energy transfer, those two cases a sometimes called 2:1 and 1:2 internal resonances, respectively) and that leads to a significant reduction of the amplitude of the driven mode. Moreover, a saturation phenomenon is theoretically predicted in the first case, for which the amplitude of the driven mode becomes independent of the forcing amplitude above a threshold, whereas in the second case, a quasi-periodic regime is obtained at resonance [43]. This leads to the idea of intentionally designing a resonant absorber with quadratic nonlinearities tuned to half the frequency of one mode of the primary structure, to beneficiate of the saturation phenomenon. In mechanical systems, this leads to the concept of autoparametric vibration absorbers, firstly proposed in [44] and addressed in many contributions since then (see [45,46] and references therein). The use of a 2:1 internal resonance to design an electromechanical control system has been proposed in many works. A first family of works proposes the vibration reduction of an elastic beam by the active control of the rotation of a direct current (DC) motor (see [47,48] in which the controller is an analog electronic circuit made of multipliers). Then, this technique has been extended to piezoelectric actuators in [49] with also an analog circuit with multipliers. Then, the same concept has been applied with a real time digital controller to several structures (a beam and a truss in [50] and a triangular panel in [51]), with design guidelines exposed in [52]. The same authors also tried a 1:2:4 internal resonance in [53].

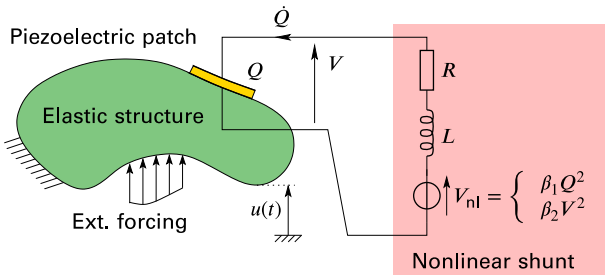

Fig. 1. Nonlinear shunt circuit.

All the above internal resonance based contributions can be related to active control. Indeed, they rely on the use of separate sensor and actuator linked with a controller (analog or digital), in which the nonlinearities and the additional degree of freedom are implemented and tuned. To our knowledge, no attempt on implementing a 2:1 internal resonance with a piezoelectric shunt has been published and this article aims at filling this gap. It is worth citing that other internal resonances have been tested: a 1:1 internal resonance in [54] as well as in the already considered NES contribution [20]. A 1:3 internal resonance between two modes of a PZT cantilever beam has been investigated in [55]. It is also worth citing [56,57], which propose strategies to implement electrical circuits analog to particular nonlinear oscillators, using multipliers.

In this paper, we propose a new semi-passive vibration attenuation approach based on a nonlinear piezoelectric shunt. Indeed, we test the simple idea of connecting, thanks to a piezoelectric transducer, a linear vibrating structure to a resonant electronic circuit in which a quadratic nonlinearity is intentionally introduced. We then add a new vibration mode in the system, that can be tuned to obtain a 2:1 internal resonance. We target creating a nonlinear antiresonance in place of the resonance of the mechanical mode as well as a saturation phenomenon. We also test two type of quadratic nonlinearities: one which is equivalent to a nonlinear capacitor, for which the electric charge is proportional to the square of the voltage, and a second one which is simply a voltage source proportional to the square of the voltage at the terminals of the piezoelectric element. In this paper, we restrict ourselves to the theory, the experimental proof of concept being postponed to an incoming article.

The outline of this paper follows. In Section 2, a model of the mechanical structure coupled to the nonlinear electric circuit is proposed, leading to a reduced model composed of two electromechanical modes coupled by quadratic terms. In Section 3, closed form approximated expressions for the amplitude and the phases of the two modes are obtained with the method of multiple scales (MMS) and the effect of several design parameters is studied. In Section 4, those results are compared to a reference solution obtained by a numerical continuation method to analyze the effect of the non-resonant nonlinear terms of the system. In Section 5, the results are applied to design a test case of a nonlinear piezoelectric absorber coupled to the first bending mode of a cantilever beam with piezoelectric patches. Some general guidelines are given in the last two sections.

2. Governing equations

We consider an arbitrary elastic structure subjected to a mechanical harmonic excitation and connected to a nonlinear resonant shunt circuit through a piezoelectric element, as shown in Fig. 1. If we discretize the displacement field of the elastic structure in a finite-element context, the equations of motions can be written [58]:

$$\boldsymbol{M}\ddot{\boldsymbol{u}} + \boldsymbol{K}\boldsymbol{u} + \boldsymbol{K}_c V = \boldsymbol{F}\cos\Omega t, \tag{1a}$$

$$C_{\text{p}} V - Q - \boldsymbol{K}_c^{\text{T}}\boldsymbol{u} = 0, \tag{1b}$$

$$V + L\ddot{Q} + R\dot{Q} + V_{\text{nl}} = 0, \tag{1c}$$

where $\boldsymbol{u}(t)$ is the mechanical displacement vector of size $N \in \mathbb{N}$ at time t, $V(t)$ is the voltage at the terminals of the piezoelectric element, $Q(t)$ is the charge in one of its electrodes, $\boldsymbol{M}$ and $\boldsymbol{K}$ are the mass and stiffness matrices, of size $N \times N$, $\boldsymbol{K}_c$ is the electromechanical coupling vector, of size N, $\boldsymbol{F}$ is the external excitation vector, of size N, Ω is the driving frequency, C_{p} is the blocked capacitance of the piezoelectric patch, L and R are the inductance and the resistance in the shunt circuit and $V_{\text{nl}}(t)$ represents the nonlinear voltage added to the shunt circuit.

We propose in this text to investigate the following two choices for V_{nl}:

$$\begin{cases} \beta_1 Q^2, & \text{(a)} \\ \beta_2 V^2, & \text{(b)} \end{cases} \tag{2}$$

where β_i $(i = 1, 2)$ are constant parameters. The first case, Eq. (2)a, can be viewed as a nonlinear capacitor for which the inverse of its capacitance C_{nl} depends linearly on the amplitude of the charge: $V_{\text{nl}} = Q/C_{\text{nl}}$ with $C_{\text{nl}} = 1/(\beta_1 Q)$. The unit of β_1 is V/C^2. This choice is driven by the mechanical nonlinear absorbers, for which their stiffness is nonlinear. The second case, Eq. (2)b, is simply a voltage source that is proportional to the square of the voltage $V(t)$ at the terminals of the piezoelectric patch, since in practice this voltage is easily monitored. The units of β_2 is V^{-1}. Those kind of nonlinearities can be obtained in practice by analog circuits with multipliers [20] or with a digital real time controller [26]. In the following, to simplify the mathematical expressions, β will be written with no index when not necessary.

2.1. Modal expansion

We consider the natural modes $(\breve{\omega}_i, \boldsymbol{\Phi}_i)$, $i = 1, \dots, N$, of the mechanical structure with the piezoelectric element in short circuit ($V = 0$), solutions of:

$$\left(\boldsymbol{K} - \breve{\omega}_i^2 \boldsymbol{M}\right) \boldsymbol{\Phi}_i = \boldsymbol{0}. \tag{3}$$

We expand the mechanical displacement vector on this modal basis, truncated to the ith mode only:

$$\boldsymbol{u}(t) = \boldsymbol{\Phi}_i q_i(t), \tag{4}$$

where $q_i(t)$ is the ith modal coordinate. This one mode assumption is valid as long as the other modes natural frequencies are far enough from $\breve{\omega}_i$ and from internal resonance relations with $\breve{\omega}_i$. The initial problem (1)a,b is then equivalent to, for all $i = 1, \dots, N$:

$$\ddot{q}_i + \breve{\omega}_i^2 q_i + \frac{\theta_i}{m_i} V = \frac{F_i}{m_i} \cos \Omega t, \tag{5a}$$

$$C_{\mathrm{p}i} V - Q - \theta_i q_i = 0 \tag{5b}$$

where $m_i = \boldsymbol{\Phi}_i^{\mathrm{T}} \boldsymbol{M} \boldsymbol{\Phi}_i$ is the ith modal mass, $F_i = \boldsymbol{\Phi}_i^{\mathrm{T}} \boldsymbol{F}$ is the ith modal forcing and $\theta_i = \boldsymbol{\Phi}_i^{\mathrm{T}} \boldsymbol{K}_c$ is the ith modal piezoelectric coupling coefficient. As explained in [59], $C_{\mathrm{p}i}$ is the effective capacitance of the piezoelectric patch in the vicinity of the ith resonance, which takes into account the static effect of all the other modes than the ith one. The above one degree of freedom model is then valid for a resonant motion of the system around its ith mode, namely by forcing around its natural frequency ($\Omega \simeq \omega_i$).

Using Eq. (5)b to eliminate the piezoelectric voltage V in Eqs. (5)a and (1)c, one obtains a problem in term of (q_i, Q) as unknowns:

$$\ddot{q}_i + 2\xi_i \hat{\omega}_i \dot{q}_i + \hat{\omega}_i^2 q_i + \frac{\theta_i}{m_i C_{\mathrm{p}i}} Q = \frac{F_i}{m_i} \cos \Omega t, \tag{6a}$$

$$\ddot{Q} + 2\xi_e \omega_e \dot{Q} + \omega_e^2 Q + \frac{\theta_i}{L C_{\mathrm{p}i}} q_i + \frac{V_{nl}}{L} = 0, \tag{6b}$$

where $\hat{\omega}_i^2 = \omega_i^2 + \theta_i^2/(C_{\mathrm{p}i} m_i)$ is an approximation (because of the one mode expansion) of the ith open circuit natural frequency. A mechanical modal viscous damping term of factor ξ_i has been added. In addition, the electrical natural frequency and damping factor are defined by:

$$\omega_e = \frac{1}{\sqrt{L C_{\mathrm{p}i}}}, \quad \xi_e = \frac{R}{2} \sqrt{\frac{C_{\mathrm{p}i}}{L}} \tag{7}$$

We also define the dimensionless electromechanical modal coupling factor (EMMCF) of the ith mode as:

$$k_i^2 = \frac{\hat{\omega}_i^2 - \breve{\omega}_i^2}{\hat{\omega}_i^2} = \frac{\theta_i^2}{\hat{\omega}_i^2 C_{\mathrm{p}i} m_i}. \tag{8}$$

Notice that its denominator is the open circuit natural frequency, following the IEEE standard [60] and because it simplifies the upcoming calculations. This is a different choice than in [58], where the short-circuit natural frequency was chosen, which gives a slightly different value of the EMMCF.

To simplify the writing of the governing equations (6)a,b, we define the following parameters:

$$\tau = \hat{\omega}_i t, \quad \bar{q}_i = \sqrt{m_i} q_i, \quad \bar{Q} = \sqrt{L} Q, \quad r_i = \frac{\omega_e}{\hat{\omega}_i}, \tag{9a}$$

$$\bar{F}_i = \frac{F_i}{\hat{\omega}_i^2 \sqrt{m_i}} \quad \bar{V}_{\mathrm{nl}} = \frac{V_{\mathrm{nl}}}{\hat{\omega}_i^2 \sqrt{L}} \quad \bar{\Omega} = \frac{\Omega}{\hat{\omega}_i} \tag{9b}$$

in order to obtain:

$$\ddot{\bar{q}}_i + 2\xi_i \dot{\bar{q}}_i + \bar{q}_i + k_i r_i \bar{Q} = \bar{F}_i \cos \bar{\Omega} \tau, \tag{10a}$$

$$\ddot{\bar{Q}} + 2\xi_e r_i \dot{\bar{Q}} + r_i^2 \bar{Q} + k_i r_i \bar{q}_i + \bar{V}_{\mathrm{nl}} = 0, \tag{10b}$$

where the derivatives in Eq. (10) are with respect to the dimensionless time τ. The time has been rescaled by the open circuit natural frequency $\hat{\omega}_i$ and we use a special scaling of the unknowns, so that $(\bar{q}_i, \bar{Q})$ share the same dimension ($\mathrm{m\,kg^{1/2}}$), to obtain the same coupling parameter $k_i r_i$ in both equations, with r_i the ratio of the electrical and mechanical natural frequencies. To prove that $(\bar{q}_i, \bar{Q})$ share the same dimension, remember that energy units can be equivalently J, N m or C V. Since the time τ is dimensionless, the units of $\bar{F}_i$ and $\bar{V}_{nl}$ are the same as $(\bar{q}_i, \bar{Q})$: $\mathrm{m\,kg^{1/2}}$.

2.2. Electro-mechanical modal expansion

The two degrees of freedom $(\bar{q}_i, \bar{Q})$ of Eq. (10)a,b are linearly coupled because of the piezoelectric coupling k_i. It is then possible to obtain a new system with diagonal linear part by expanding the unknowns onto the electromechanical modal basis $(\omega_k, \boldsymbol{\Psi}_k)$ of

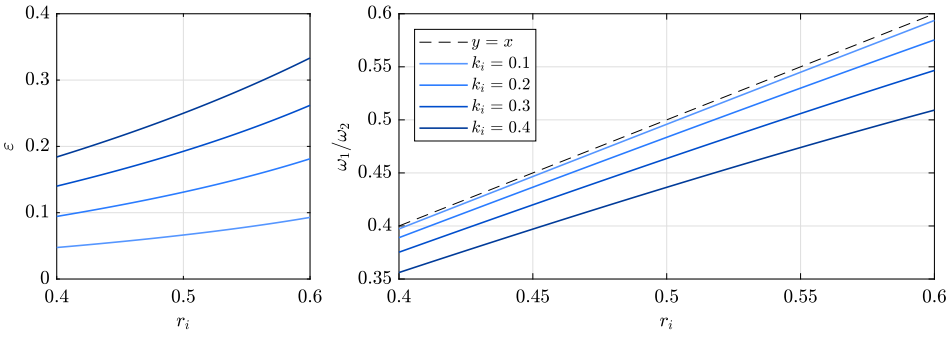

Fig. 2. (left) Mode shape parameter ε (from Eq. (14)) and (right) electromechanical natural frequency ratio ω_1/ω_2 (from Eqs. (12)) as a function of the frequency ratio r_i, for various values of the EMMCF k_i, as specified.

the problem, solution of:

$$\left(\bar{\boldsymbol{K}} - \omega_k^2 \boldsymbol{I}\right) \boldsymbol{\Psi}_k = \boldsymbol{0}, \quad k = 1, 2, \quad \bar{\boldsymbol{K}} = \begin{pmatrix} 1 & k_i r_i \\ k_i r_i & r_i^2 \end{pmatrix}. \tag{11}$$

Solving this eigenproblem, one obtains:

$$\omega_1^2 = \frac{1 + r_i^2 - \sqrt{\Delta}}{2}, \quad \omega_2^2 = \frac{1 + r_i^2 + \sqrt{\Delta}}{2} \tag{12}$$

with $\Delta = (1 - r_i^2)^2 + 4k_i^2 r_i^2$ and

$$\boldsymbol{\Psi}_1 = \begin{pmatrix} -\varepsilon \\ 1 \end{pmatrix}, \quad \boldsymbol{\Psi}_2 = \begin{pmatrix} 1 \\ \varepsilon \end{pmatrix}, \tag{13}$$

with

$$\varepsilon = \frac{2k_i r_i}{1 - r_i^2 + \sqrt{\Delta}}. \tag{14}$$

Then, following the modal expansion:

$$\begin{pmatrix} \bar{q}_i(\tau) \\ \bar{Q}(\tau) \end{pmatrix} = \sum_{k=1}^{2} \boldsymbol{\Psi}_k x_k(\tau), \tag{15}$$

one obtains the following change of variables:

$$\bar{q}_i(\tau) = -\varepsilon x_1(\tau) + x_2(\tau), \tag{16a}$$

$$\bar{Q}(\tau) = x_1(\tau) + \varepsilon x_2(\tau). \tag{16b}$$

Since the coupling factor k_i is small compared to 1, ε is also small compared to 1, which is illustrated in Fig. 2(left). For instance, for $r_i = 0.5$ and $k_i = 0.1$, $\varepsilon = 0.07$. Eq. (16) then shows that the dominant effect of x_1 and x_2 will be respectively on $\bar{Q}$ and $\bar{q}$. Based on that, $\boldsymbol{\Psi}_1$ and $\boldsymbol{\Psi}_2$ will be designated as the electrical and mechanical modes respectively.

As for the frequencies, ω_1 is close to the dimensionless electrical frequency $\omega_e/\hat{\omega}_i = r_i$ and ω_2 is close to the dimensionless mechanical frequency $\hat{\omega}_i/\hat{\omega}_i = 1$. In particular, if the EMMCF k_i is zero, there is no electromechanical coupling, the system (10)a,b is uncoupled and $\varepsilon = 0$, $\omega_1 = r_i$ and $\omega_2 = 1$. To quantify the effect of k_i on the electromechanical eigenmodes shift with respect to purely electrical and mechanical modes, Fig. 2(right) shows the natural frequency ratio ω_1/ω_2 as a function of r_i for various values of k_i. One can see that k_i imposes a detuning between the electromechanical natural frequency ratio ω_1/ω_2 with respect to r_i. In particular, to obtain a specified tuning ω_1/ω_2 (for instance 0.5 to obtain a 2:1 internal resonance), r_i has to be slightly overtuned ($r_i > \omega_1/\omega_2$).

Regarding the nonlinear voltage V_{nl}, considering Eq. (5)b, we write it in the following form:

$$V_{nl} = \beta(\kappa_1 Q + \kappa_2 q_i)^2, \tag{17}$$

where $(\kappa_1, \kappa_2) = (1, 0)$ to verify Eq. (2)a and $(\kappa_1, \kappa_2) = (1, \theta_i)/C_{\mathrm{p}i}$ to verify Eq. (2)b.

By substituting Eq. (15) in Eqs. (10), multiplying by $\boldsymbol{\Psi}_k^T$, using the orthogonality properties of the electromechanical eigenmodes and the form of V_{nl} defined in Eq. (17), and by considering that the modal mass is $1 + \varepsilon^2 \simeq 1$ because $\varepsilon \ll 1$, the following can be written:

$$\ddot{x_1} + 2\mu_1 \dot{x_1} + 2\mu_{12} \dot{x_2} + \omega_1^2 x_1 + \Lambda_1 x_1^2 + \Lambda_2 x_1 x_2 + \Lambda_3 x_2^2 = f_1 \cos \bar{\Omega} \tau, \tag{18a}$$

$$\ddot{x_2} + 2\mu_{12}\dot{x_1} + 2\mu_2\dot{x_2} + \omega_2^2 x_2 + \Lambda_4 x_1^2 + \Lambda_5 x_1 x_2 + \Lambda_6 x_2^2 = f_2 \cos\bar{\Omega}\tau. \tag{18b}$$

In the above system, the new (dimensionless) damping terms are defined as:

$$\mu_1 = \xi_e r_i - \xi_i \varepsilon^2, \quad \mu_{12} = (\xi_e r_i - \xi_i)\varepsilon,$$
$$\mu_2 = \xi_i + \xi_e r_i \varepsilon^2 \tag{19}$$

and the forcing terms are:

$$f_1 = -\varepsilon \bar{F}_i, \quad f_2 = \bar{F}_i, \tag{20}$$

with units $\mathrm{m\,kg}^{1/2}$. The nonlinear coefficients of Eq. (18) write:

$$\begin{aligned} \Lambda_1 &= \lambda_1 - \lambda_2\varepsilon + \lambda_3\varepsilon^2 & \Lambda_4 &= \varepsilon\Lambda_1 \\ \Lambda_2 &= 2\lambda_1\varepsilon + \lambda_2(1-\varepsilon^2) - 2\lambda_3\varepsilon & \Lambda_5 &= \varepsilon\Lambda_2 \\ \Lambda_3 &= \lambda_1\varepsilon^2 + \lambda_2\varepsilon + \lambda_3 & \Lambda_6 &= \varepsilon\Lambda_3 \end{aligned} \tag{21}$$

where

$$\lambda_1 = \beta\kappa_1^2 r_i^3 \hat{\omega}_i C_{\mathrm{p}i}^{3/2}, \quad \lambda_2 = \frac{2\beta\kappa_1\kappa_2 r_i^2 C_{\mathrm{p}i}}{\sqrt{m_i}}, \tag{22a}$$

$$\lambda_3 = \frac{\beta\kappa_2^2 r_i \sqrt{C_{\mathrm{p}i}}}{m_i \hat{\omega}_i}. \tag{22b}$$

The common units of all those coefficients are $\mathrm{m}^{-1}\,\mathrm{kg}^{-1/2}$.

Then, for the choice of Eq. (2)a, $(\kappa_1, \kappa_2) = (1, 0)$ and the λ_i write:

$$\lambda_1 = \beta_1 r_i^3 \hat{\omega}_i C_{\mathrm{p}i}^{3/2}, \quad \lambda_2 = \lambda_3 = 0. \tag{23}$$

For the choice of Eq. (2)b, $(\kappa_1, \kappa_2) = (1, \theta_i)/C_{\mathrm{p}i}$ and:

$$(\lambda_1, \lambda_2, \lambda_3) = (r_i^3, 2r_i^2 k_i, r_i k_i^2)\lambda_0, \quad \lambda_0 = \frac{\beta_2 \hat{\omega}_i}{\sqrt{C_{\mathrm{p}i}}}. \tag{24}$$

3. Analytical results

3.1. Multiple scale solution

In this section, closed form expressions governing the response of the electromechanical modal system of Eqs. (18)a,b is given. This is done in order to study the performance of the vibration absorber and the effect of the design parameters, given later in this section, that could be controlled to enhance the vibration absorber performance.

We restrict ourselves to the case of a 2:1 internal resonance with $\omega_2 \simeq 2\omega_1$. This leads to neglect in Eqs. (18)a,b the effect of the non-resonant terms of coefficients Λ_1, Λ_3, Λ_5, and Λ_6 on the dynamics. This is motivated by the normal form theory, which proves that only the resonant terms (of coefficients Λ_2 and Λ_4) have an effect at first order (see [61,62]). We are also interested in the case for which the energy is injected mainly to the mechanical (2nd. mode) and transferred to the electrical (1st. mode) because of the nonlinear term. We then consider a pure forcing of the second (mechanical, high frequency) oscillator and neglect εf_1 with respect to f_2, since $\varepsilon \ll 1$. Finally, the damping coupling terms of coefficient μ_{12} are neglected. This is motivated because $\varepsilon \ll 1$ and also because the damping is considered small: $\mu_1, \mu_2 \ll 1$. In this case, it can be shown that the non diagonal terms have a negligible effect on the dynamics [63].

Consequently, for the analytical results, we consider the following system:

$$\ddot{x_1} + 2\epsilon\mu_1\dot{x_1} + \omega_1^2 x_1 + \epsilon\Lambda_2 x_1 x_2 = 0 \tag{25a}$$

$$\ddot{x_2} + 2\epsilon\mu_2\dot{x_2} + \omega_2^2 x_2 + \epsilon\Lambda_4 x_1^2 = f_2 \cos\bar{\Omega}\tau \tag{25b}$$

where a bookkeeping parameter ϵ has been added to scale the terms of the equation before applying the perturbation method. Following the multiple scales method, as fully described in [64], the two modal coordinates $x_1(\tau)$ and $x_2(\tau)$ are approximated at first order by:

$$x_1 = a_1 \cos\left(\frac{\bar{\Omega}}{2}\tau - \frac{\gamma_1 + \gamma_2}{2}\right), \tag{26a}$$

$$x_2 = a_2 \cos(\bar{\Omega}\tau - \gamma_2). \tag{26b}$$

where the amplitudes a_1 and a_2 and the phase angles γ_1 and γ_2 are the solutions of the following modulation equations:

$$a_1' = -\mu_1 a_1 - \frac{\Lambda_2 a_1 a_2}{4\omega_1}\sin\gamma_1, \tag{27a}$$

$$\frac{1}{2}(\gamma_1' + \gamma_2')a_1 = \frac{\sigma_1 + \sigma_2}{2}a_1 - \frac{\Lambda_2 a_1 a_2}{4\omega_1}\cos\gamma_1, \tag{27b}$$

$$a_2' = -\mu_2 a_2 + \frac{\Lambda_4 a_1^2}{4\omega_2}\sin\gamma_1 + \frac{f_2}{2\omega_2}\sin\gamma_2, \tag{27c}$$

$$\gamma_2' a_2 = \sigma_1 a_2 - \frac{\Lambda_4 a_1^2}{4\omega_2}\cos\gamma_1 + \frac{f_2}{2\omega_2}\cos\gamma_2, \tag{27d}$$

where $\circ' = \partial\circ/(\partial\epsilon\tau)$ is the derivative with respect to the slow time scale and

$$\epsilon\sigma_1 = \bar{\Omega} - \omega_2, \quad \epsilon\sigma_2 = \omega_2 - 2\omega_1, \tag{28}$$

are the two detuning parameters, which express respectively the nearness of the driving frequency to the mechanical resonance $\bar{\Omega} \simeq \omega_2$ and the detuning of the two natural frequency with respect to the exact internal resonance, which would be $\omega_2 = 2\omega_1$.

The response amplitudes a_1 and a_2 and the phase angles γ_1 and γ_2 are estimated using the fixed-point solution of the above dynamical system, i.e with $a_1' = a_2' = \gamma_1' = \gamma_2' = 0$. It leads to two kinds of solutions (see e.g. [64,65] for details):

- An *uncoupled (U) solution*, for which only the directly excited mode responds ($a_2 \neq 0, a_1 = 0$). This is the trivial linear solution, which writes:

$$a_2^U = \frac{f_2}{2\omega_2\sqrt{\sigma_1^2 + \mu_2^2}}, \quad \gamma_2^U = \arctan\frac{\mu_2}{-\sigma_1}, \tag{29a}$$

$$a_1^U = 0. \tag{29b}$$

- A *coupled (C) solutions*, for which the energy is transferred from the second (directly excited) oscillator to the first one thanks to the nonlinear terms. In this case, $a_1 \neq 0$ and $a_2 \neq 0$ are obtained by:

$$a_2^C = \frac{2\omega_1}{|\Lambda_2|}\sqrt{4\mu_1^2 + (\sigma_1 + \sigma_2)^2}, \tag{30a}$$

$$a_1^C = 2\sqrt{-\Gamma_1 \pm \sqrt{\frac{f_2^2}{4\Lambda_4^2} - \Gamma_2^2}}, \tag{30b}$$

$$\gamma_1^C = \arctan\frac{-2\mu_1}{\sigma_1 + \sigma_2}\ [2\pi], \tag{30c}$$

$$\gamma_2^C = \arctan\frac{2(\Lambda_4\mu_1\omega_1 a_1^2 + \Lambda_2\mu_2\omega_2 a_2^2)}{(\sigma_1 + \sigma_2)\Lambda_4\omega_1 a_1^2 - 2\sigma_1\Lambda_2\omega_2 a_2^2}\ [2\pi], \tag{30d}$$

where $[2\pi]$ means modulo 2π and with

$$\Gamma_1 = \frac{2\omega_1\omega_2}{\Lambda_2\Lambda_4}\left[2\mu_1\mu_2 - \sigma_1(\sigma_1 + \sigma_2)\right], \tag{31a}$$

$$\Gamma_2 = \frac{2\omega_1\omega_2}{\Lambda_2\Lambda_4}\left[2\sigma_1\mu_1 + \mu_2(\sigma_1 + \sigma_2)\right]. \tag{31b}$$

In all the above expressions, the phases γ_1 and γ_2 are strictly defined since their sine and cosine are given in the dynamical system (27). The formula including $\arctan(b/a)$ must be understood as the angle of the complex number $a+ib$, computed numerically with the function $\mathrm{atan2}(b, a)$ in most numerical languages.

3.2. Typical response

A stability analysis of the fixed points of the slow scale dynamical system (27) shows that there exists an instability region in the plane (σ_1, a_2) in which the U-solution is unstable [65]. Namely, it is the case as long as:

$$a_2 \geq \mathcal{L}(\sigma_1), \quad \mathcal{L}(\sigma_1) = \frac{2\omega_1}{|\Lambda_2|}\sqrt{4\mu_1^2 + (\sigma_1 + \sigma_2)^2}. \tag{32}$$

The analytical expression of $\mathcal{L}(\sigma_1)$ is exactly the same than $a_2^C(\sigma_1)$ which means that the boundary of the instability region coincides with the C-solution for the directly excited mode a_2.

Fig. 3 shows the typical frequency response of the system when driven at constant f_2 and sweeping around the second oscillator resonance $\bar{\Omega} \simeq \omega_2$ ($\sigma_1 \simeq 0$). At the crossing points between the amplitude of the U-solution and the instability region, two subcritical pitchfork bifurcations (points "PF" in Fig. 3) give rise to an unstable C-solution, which becomes stable after saddle–node bifurcations (points "SN"). This stable C-solution is characterized by a non-zero response of the low-frequency (electrical) mode, which oscillates at the subharmonic $\bar{\Omega}/2$ (see Eq. (26)a). In the frequency band between the two pitchfork bifurcations, the resonance of the driven (mechanical) mode is replaced by a low amplitude response, *which shows a minimum at exactly* $\bar{\Omega} = 2\omega_1$ (Point *A* of Fig. 3, $\sigma_1 = -\sigma_2$, see Eq. (30)a), that can be viewed as a *nonlinear antiresonance*. The phase γ_1 is exactly $3\pi/2\,[2\pi]$ at this point (see Eq. (30)c). The main idea of the article is to take advantage of this nonlinear antiresonance to reduce de vibrations of a given resonance.

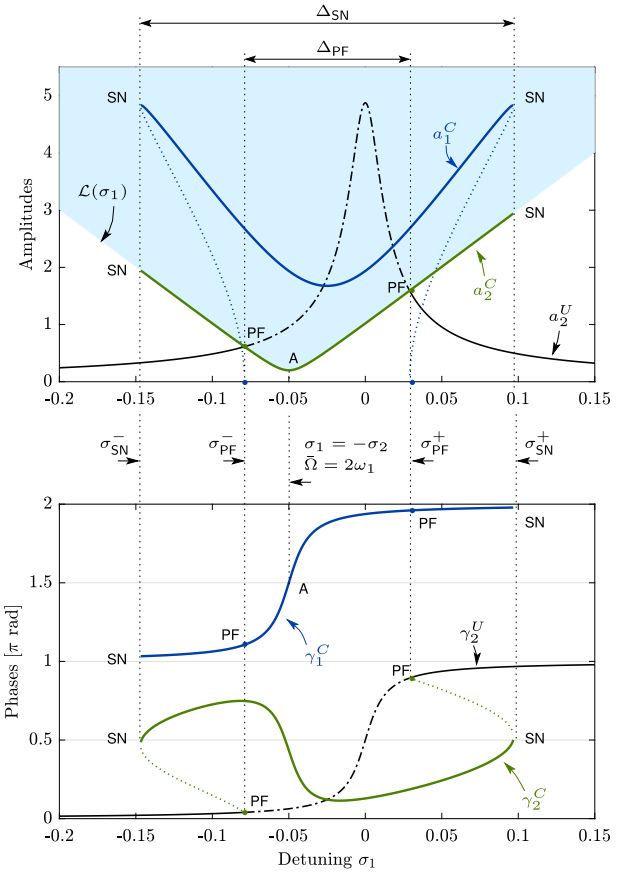

Fig. 3. Typical frequency response of Eqs. (25) obtained with the MS method: amplitude a_1, a_2 and phases γ_1, γ_2 as a function of the detuning σ_1 for a constant forcing f_2. The parameters are $\Lambda_2 = \Lambda_4 = 0.1$, $\mu_1 = 0.005$, $\mu_2 = 0.01$, $f_2 = 0.2$, $\sigma_2 = 0.05$. "PF"means pitchfork bifurcation; "SN"means saddle–node bifurcation; superscript U refers to the uncoupled solution (in black) whereas superscript C refers to the coupled solution (in blue for (a_1, γ_1) and in green for (a_2, γ_2)). The blue shaded area depicts the instability region for a_2^U. Dotted and dash-dotted lines depict unstable branches.

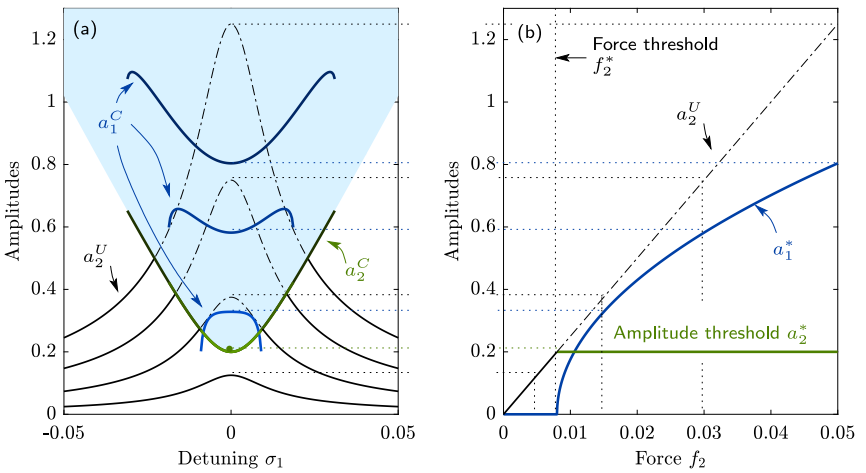

Fig. 4. Typical response of Eqs. (25) obtained with the MS method for a perfect tuning $\sigma_2 = 0$ ($\omega_2 = 2\omega_1$). (a) amplitudes a_1 and a_2 as a function of the detuning σ_1 for several values of the forcing f_2 ($f_2 \in \{0.005; 0.015; 0.03; 0.05\}$); (b) amplitudes a_1 and a_2 for a forcing at the antiresonance ($\sigma_1 = 0$, $\bar{\Omega} = \omega_2$, as a function of the forcing f_2. The numerical values are $\Lambda_2 = \Lambda_4 = 0.1$, $\mu_1 = 0.005$, $\mu_2 = 0.01$. Superscript U refers to the uncoupled solution (in black) whereas superscript C refers to the coupled solution (in blue for a_1 and in green for a_2). The blue shaded area depicts the instability region for a_2^U.

By tuning the electrical mode eigenfrequency exactly to half the one of the mechanical mode, $\omega_1 = \omega_2/2$ ($\sigma_2 = 0$), it is then possible to replace the linear resonance of the mechanical mode by the nonlinear antiresonance. Since the energy transfer to the electrical mode is nonlinear, the performances are dependent on the excitation level. This is illustrated in Fig. 4 in which several response curves are shown for increasing forcing levels f_2. For low values of f_2, the linear resonance (the U-solution) is below the instability region and no energy transfer occurs. For the perfect tuning, $\sigma_2 = 0$, the minimum value f_2^* of the force necessary to create the energy transfer is obtained by equating a_2 between Eqs. (29)a and (30)a with $\sigma_1 = \sigma_2 = 0$:

$$f_2^* = \frac{8\omega_1\omega_2\mu_1\mu_2}{|\Lambda_2|} = \frac{4\omega_2^2\mu_1\mu_2}{|\Lambda_2|}. \tag{33}$$

Above this threshold ($f_2 > f_2^*$), the coupled regime occurs and an interesting result is that the amplitude a_2^C of the driven mode is independent of the forcing level f_2 instead of being proportional to it, which is observed before the threshold. This leads to a *saturation phenomenon* for a_2^C, shown in Fig. 4(b), with the constant amplitude:

$$a_2^* = \frac{f_2^*}{2\omega_2\mu_2} = \frac{4\omega_1\mu_1}{|\Lambda_2|} = \frac{2\omega_2\mu_1}{|\Lambda_2|}, \tag{34}$$

equal to the one at the antiresonance.

On the contrary, the amplitude of the electrical mode increases with a square root dependence on the forcing amplitude at the antiresonance, also shown in Fig. 4(b). It can be written:

$$a_1^* = \sqrt{\frac{2}{|\Lambda_4|}(f_2 - f_2^*)}, \tag{35}$$

obtained by setting $\sigma_1 = \sigma_2 = 0$ in Eqs. (31) and (30)b.

Still in the special case of perfect tuning ($\sigma_2 = 0$), the values of the pitchfork bifurcation frequencies can be obtained by equating a_2 between Eqs. (29)a and (30)a with $\sigma_2 = 0 \Rightarrow \omega_1 = \omega_2/2$ (or equivalently by enforcing $a_1^C = 0$ in Eq. (30)b), as:

$$\sigma_{\mathrm{PF}}^+ = \sqrt{\frac{\sqrt{(4\mu_1^2 - \mu_2^2)^2 + \dfrac{f_2^2\Lambda_2^2}{\omega_2^4}} - 4\mu_1^2 - \mu_2^2}{2}}, \tag{36a}$$

$$\sigma_{\mathrm{PF}}^- = -\sigma_{\mathrm{PF}}^+, \quad \Delta_{\mathrm{PF}} = 2\sigma_{\mathrm{PF}}^+. \tag{36b}$$

where Δ_{PF} characterizes the instability bandwidth (see Fig. 3). Moreover, the values of the saddle–node bifurcations frequencies are obtained by enforcing to zero the radicand of the inner square root of a_1^C in Eq. (30)b:

$$\sigma_{\mathrm{SN}}^+ = \frac{f_2|\Lambda_2|}{\omega_2^2(2\mu_1 + \mu_2)}, \quad \sigma_{\mathrm{SN}}^- = -\sigma_{\mathrm{SN}}^+, \quad \Delta_{\mathrm{SN}} = 2\sigma_{\mathrm{SN}}^+, \tag{37}$$

where Δ_{SN} characterizes the full bandwidth of the response (see Fig. 3).

One idea could be to use Δ_{SN} and Δ_{PF} as design parameters: one could think of adjusting the shunt parameters μ_1 and Λ_2 to obtain a vibration reduction bandwidth Δ_{PF} as large as possible while minimizing the amplitude of the two lateral "wings" of the frequency response by decreasing Δ_{SN} as much as possible. However, it should not be forgotten that the response of the system is nonlinear and forcing amplitude dependent. In particular, Δ_{SN} and Δ_{PF} are increasing functions of the forcing f_2. Consequently, by looking at Fig. 4, it is clear that tailoring Δ_{PF} and Δ_{SN} is possible at a given forcing amplitude, but that the particular shape of the frequency response will by lost for higher forcing amplitudes.

3.3. Effect of the parameters

In order to propose guidelines for the design of the nonlinear shunt, this section addresses the effect of the parameters of the system: the detuning $\sigma_2 = \omega_2 - 2\omega_1$ (from now on, we drop the bookkeeping parameter ϵ in the equations, meaning that the small parameters μ_1, μ_2, Λ_2, Λ_4, σ_1, σ_2 are now considered with there nominal values, assumed small, to guarantee the validity of the multiple scale developments), the excitation level f_2, the damping parameters (μ_1, μ_2) and the coefficients of the quadratic terms (Λ_2, Λ_4). In all this section, we assume that $\omega_1 = 1$, with no loss of generality since one can rescale the time in Eqs. (25) and show that the topology of the response curves does not depend on ω_1. The effect of f_2 has been investigated in the previous section and we consider here the other parameters.

The effect of the detuning parameter σ_2 is to shift the antiresonance frequency ($\sigma_2 > 0$ (resp. $\sigma_2 < 0$) shifts it to the lower (resp. upper) frequencies) and to desymmetrize the shape of the frequency response. In particular, a perfect tuning ($\sigma_2 = 0$, $\omega_2 = 2\omega_1$) gives symmetrical curves with respect to the vertical axis $\sigma_1 = 0$ ($\bar{\Omega} = \omega_2$). This can be inferred by comparing Fig. 3 (obtained with $\sigma_2 = 0.05$) and Fig. 4(a) (with a perfect tuning, $\sigma_2 = 0$). In practice, a perfect tuning appears to be optimal since it guarantees the tuning of the antiresonance in place of the linear resonance. This case is solely investigated in the remaining of the section.

By observing Eqs. (32)–(37), one can conclude that Λ_2 and μ_1 have a crucial effect on the system's response, since they appear in all those equations. The first effect of (Λ_2, μ_1) is on the shape of the instability region boundary $\mathcal{L}$. Following Eq. (32), if $\mu_1 = 0$, $\mathcal{L} = 2\omega_1|\sigma_1|/|\Lambda_2|$ and thus reduces to a triangle bounded by straight lines of slope $\pm 2\omega_1/|\Lambda_2|$. Consequently, increasing Λ_2 decreases

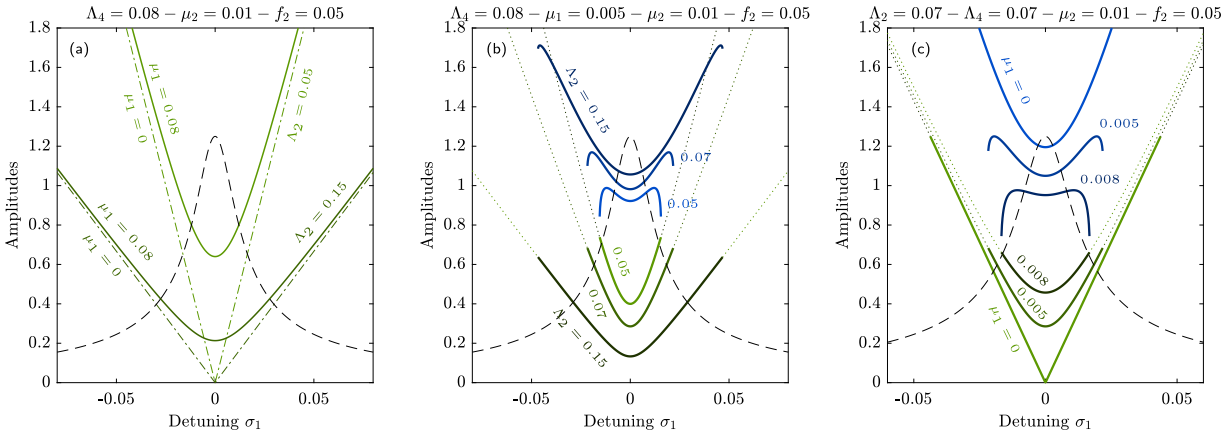

Fig. 5. Effect of variation of parameters Λ_2 and μ_1 on the system's frequency response, obtained with the MS method for a perfect tuning $\sigma_2 = 0$ ($\omega_2 = 2\omega_1$). (a) Effect of the variation of Λ_2, with $\mu_1 = 0$ and $\mu_1 \neq 0$, on the instability region $\mathcal{L}(\sigma_1)$; (b) Effect of the variation of Λ_2 on the response curves amplitudes (a_1, a_2); (c) Effect of the variation of μ_1 on the response curves amplitudes (a_1, a_2). The uncoupled solution a_2^U is in black and the coupled solutions (a_1^C, a_2^C) are respectively in blue and green.

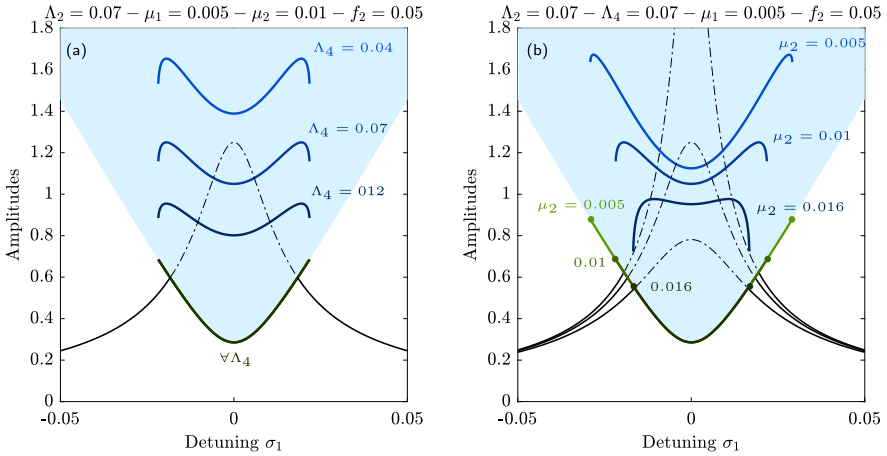

Fig. 6. Effect of variation of parameters Λ_4 and μ_2 on the system's frequency response, obtained with the MS method for a perfect tuning $\sigma_2 = 0$ ($\omega_2 = 2\omega_1$). (a) Effect of the variation of Λ_4 on the response curves amplitudes (a_1, a_2); (b) Effect of the variation of μ_2 on the response curves amplitudes (a_1, a_2). The uncoupled solution a_2^U is in black and the coupled solutions (a_1^C, a_2^C) are respectively in blue and green.

these slopes and thus widens the instability region, as illustrated in Fig. 5(a). The effect of increasing μ_1 from zero is to round the shape of the instability region at its lower end and thus to decrease its area. Since the amplitude a_2^C of the driven mode coincides with $\mathcal{L}$, the same conclusions can be drawn, as shown in Figs. 5(b, c). In particular, the parameter $|\Lambda_2|/\mu_1$ seems crucial: increasing it leads to reduce the threshold amplitude of the energy transfer (see Eqs. (33) and (34) and Fig. 5(a–c)). A zero value of (f_2^*, a_2^*) can even theoretically be obtained with a zero electrical damping ($\mu_1 = 0$). In addition, Figs. 5(b, c) illustrate the effect of (Λ_2, μ_1) on the amplitude a_1^C of the electrical mode: increasing Λ_2 and/or decreasing μ_1 increases a_1^C. As a conclusion, it is clear that increasing $|\Lambda_2|/\mu_1$ leads to improve the performances of the absorber.

On the contrary, Λ_4 appears only in the amplitude a_1 of the electrical mode. Consequently, increasing it leads to decrease a_1^C and thus to improve the absorber performance, as shown in Fig. 6(a). Finally, Fig. 6(b) illustrates the effect of the mechanical mode damping μ_2 on the system's response. Decreasing μ_2 leads to increase the amplitude of the linear resonance, but has no effect on the instability boundary $\mathcal{L}$ and the saturation amplitude a_2^*. Consequently, the less the mechanical mode is damped, the less the forcing threshold f_2^* is and the better performance the absorber has.

4. Validity of the analytical solution and design of the nonlinear absorber

In Section 3, an analytical solution of the dynamical system (18) is investigated, by canceling the non diagonal damping terms and the non-resonant terms (of coefficients Λ_i, $i = 1, 3, 5, 6$). This section is devoted to the validity of this analytical solution, by comparing it to reference numerical simulations. They are obtained with the software Manlab, that enables the numerical continuation of

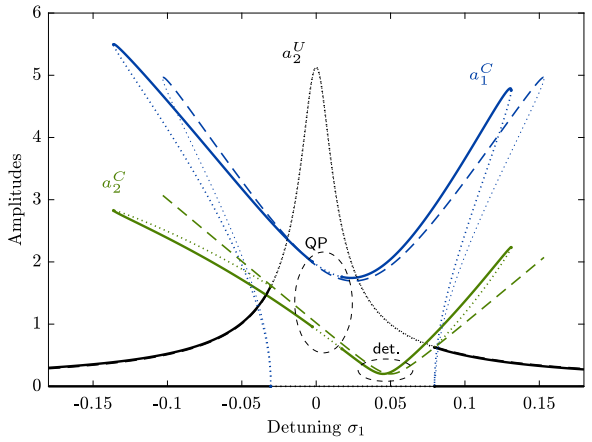

Fig. 7. Frequency response of Eqs. (25): comparison of the analytical MS solution (thin '- -') to a reference Manlab solution (thick '—') of the same system. Amplitude a_1, a_2 the detuning σ_1. The parameters are $\Lambda_2 = \Lambda_4 = 0.1$, $\mu_1 = 0.005$, $\mu_2 = 0.01$, $f_2 = 0.2$, $\sigma_2 = -0.05$. "QP" means quasi-periodic response; "det." means "detuning". The uncoupled solution a_2^U is in black and the coupled solutions (a_1^C, a_2^C) are respectively in blue and green. $H = 20$ harmonics have been considered for the Manlab HBM computations.

periodic solutions of the dynamical system. It is based on the harmonic balance method (HBM) and the asymptotic numerical method [66,67], with a special strategy to compute the branching points and the stability of the branches [42,68].

4.1. Validity of the analytical solution without the non-resonant terms

We first investigate the validity of the analytical MS solution of Eqs. (27) of the simplified dynamical system (25) in 2:1 internal resonance ($\omega_2 \simeq 2\omega_1$), by comparing it to the Manlab solution. Fig. 7 shows its frequency response with typical parameters. We can observe that the reference Manlab solution is more asymmetrical with respect to the MS solution. One interesting effect is that the frequency of the nonlinear antiresonance is slightly shifted to the low frequencies and does not appear exactly at $\bar{\Omega} = 2\omega_1$ ($\sigma_1 = -\sigma_2$). By changing the tuning of the two modes, it has been verified that this shift always appears toward the low frequencies, for any positive or negative small detuning σ_2, and that it increases with the excitation level f_2. It has also been numerically verified that the phase of the electrical mode is precisely $\gamma_1^C = 3\pi/2\,[2\pi]$ at the numerical antiresonance frequency, as predicted by the MS solution.

Another feature is the appearance of a small frequency band in which the periodic response is unstable due to Neimark–Sacker bifurcations, which leads to a quasi-periodic response. This quasi-periodic response does not appear for any values of the parameters and tends to be more prominent for large values of f_2. These Neimark–Sacker bifurcations can be predicted with the MS solution, but no close form expression is at hand since they depend on the solution of an order four polynomial [69]. We consequently decided not to show them on the MS solution plots.

4.2. Effect of non-resonant terms

We investigate in this section the effect of the non-resonant terms on the dynamics. To estimate their order of magnitude in a practical piezoelectric shunt example, we consider, as explained in Section 2, that the coupling factor k_i, and thus ε, are small compared to 1. Then, for the case of $V_{\text{nl}} = \beta_1 Q^2$ (Eqs. (2)a, (23)), one has with Eqs. (21):

$$\Lambda_1 = \lambda_1, \quad \Lambda_2 = 2\varepsilon\lambda_1, \quad \Lambda_4 = \varepsilon\lambda_1 \tag{38}$$

$$\Lambda_3 = \varepsilon^2\lambda_1, \quad \Lambda_5 = 2\varepsilon^2\lambda_1, \quad \Lambda_6 = \varepsilon^3\lambda_1. \tag{39}$$

In the other case of $V_{\text{nl}} = \beta_2 V^2$ (Eqs. (2)b, (24)), keeping the leading order in ε in Eqs. (21) conducts to $\Lambda_k \simeq \lambda_k$ for all $k = 1, 2, 3$. Then, to set the ideas, we consider numerical values: $r_i = 0.5$ and $k_i = 0.1$ leads to $\varepsilon = 0.07$ (Fig. 2). One then obtains:

$$\Lambda_1 = 0.13\lambda_0, \quad \Lambda_2 = 0.05\lambda_0, \quad \Lambda_4 = 0.009\lambda_0 \tag{40}$$

$$\Lambda_3 = 0.005\lambda_0, \quad \Lambda_5 = 0.004\lambda_0, \quad \Lambda_6 = 0.0004\lambda_0. \tag{41}$$

In both cases for the choice of V_{nl}, Λ_1 is larger than the two coefficients (Λ_2, Λ_4) of the resonant terms, with the other coefficient $(\Lambda_3, \Lambda_5, \Lambda_6)$ negligible. It is then assumed in the remaining of the section that Λ_1 is the dominant non-resonant term and we analyze its effect on the frequency response of the system, with $\Lambda_3 = \Lambda_5 = \Lambda_6 = 0$. We thus consider Eqs. (25) with an additional nonlinear term $\Lambda_1 x_1^2$ in Eq. (25)a.

As a first step, the effect of Λ_1 on the response is investigated in Fig. 8 for the perfect tuning case ($\sigma_2 = 0 \Leftrightarrow \omega_2 = 2\omega_1$). One can see that increasing Λ_1 from zero to positive values of the order of magnitude of the resonant term coefficients Λ_2 and Λ_4 leads

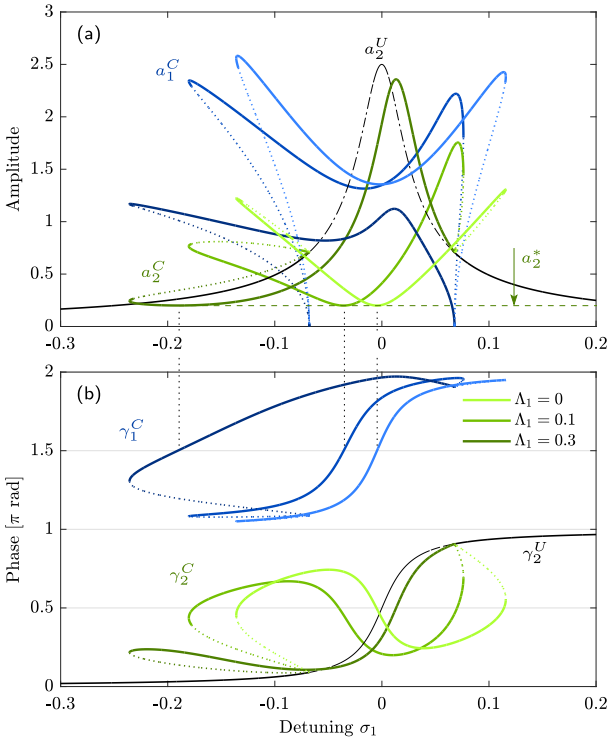

Fig. 8. Effect of variation of parameter Λ_1 on the frequency response of the complete system (18), obtained with Manlab, for a perfect tuning $\sigma_2 = 0$ ($\omega_2 = 2\omega_1$). The parameters are $\Lambda_1 \in \{0; 0.2; 0.3\}$, $\Lambda_2 = \Lambda_4 = 0.1$, $\Lambda_3 = \Lambda_5 = \Lambda_6 = 0$, $\mu_1 = 0.005$, $\mu_2 = 0.01$, $f_2 = 0.1$. The uncoupled solution (a_2^U, γ_2^U) is in black and the coupled solutions (a_1^C, γ_1^C), (a_2^C, γ_2^C) are respectively in blue and green, with a darker color as Λ_1 increases.

to a qualitative change of the shape of the response curves. Their symmetry with respect to the axis $\sigma_1 = 0$ is lost, with a kind of overall "bending" of the curves to the low frequencies and with a decreasing of the amplitude of a_1^C (blue curves). This bending seems qualitatively analogous to a softening behavior of the resonance of a Duffing oscillator. The main result is that *increasing* Λ_1 *shifts the antiresonance frequency of* a_2^C *to the low frequencies* (see the minimum of the green curves in Fig. 8(a)). It then shows that the simple tuning property of the simplified model (see Section 3.2, the antiresonance depends only on the eigenmode tuning since it is obtained exactly at $\sigma_1 = -\sigma_2$ ($\bar{\Omega} = 2\omega_1$)) is lost with a non-zero Λ_1. One can also observe that the asymmetry of the response curves due to high values of Λ_1 also increases the amplitude of the high frequency peak of the mechanical mode response a_2^C.

However, two interesting properties are kept with a non-zero Λ_1. First, the amplitude of the antiresonance seems independent of Λ_1 and thus keeps the analytical value a_2^* of Eq. (34). Secondly, the property of phase locking of $\gamma_1^C = 3\pi/2[2\pi]$ at the antiresonance seems perfectly kept. Those results have only been verified numerically by observing the minimum of a_2^C and the crossing of $\gamma_1^C = f(\sigma_1)$ curve with the horizontal $3\pi/2$ line, as seen in Fig. 8.

We now investigate the effect on the frequency response of the other parameters of the system, namely f_2, σ_2 and μ_1, with a nonzero value of the non-resonant term coefficient, chosen equal to the ones of the resonant terms ($\Lambda_1 = \Lambda_2 = \Lambda_4 = 0.1$). Figs. 9(a, b) show that increasing f_2 or decreasing μ_1 naturally increase the amplitude of the responses but also amplifies the negative effect of a non-zero Λ_1 described above, by increases the shift the antiresonance to the low frequencies. However, as seen in Fig. 9(c), it is still possible to adjust the value of the antiresonance frequency by changing the eigenmode detuning σ_2: decreasing (increasing) σ_2 from zero shifts it to the high-frequencies (low-frequencies). Moreover, one can observe in the insets of Figs. 9(a, c) that the antiresonance amplitude is still independent of f_2 and σ_2 and equal to a_2^*. Another remark is that a quasi-periodic response can also be observed for low (negative) values of σ_2, a feature already observed with $\Lambda_1 = 0$ in Fig. 7. Moreover, one can observe in Fig. 9(b) that the amplitude of a_1^C at the antiresonance seems independent of μ_1. This effect is here a particular case, a consequence of the choice of the parameters, different from the one used in Fig. 5, and not of the presence of Λ_1.

4.3. Correction of the antiresonance detuning

As seen in the previous sections and contrary to what predicted by the MS solution of the simplified model, the frequency of the antiresonance of a_2^C is clearly affected by the parameters and this effect is amplified by a non-zero value of the non-resonant term coefficient Λ_1. On the contrary, the amplitude of this antiresonance keeps its analytical value a_2^* (Eq. (34)), independent of the forcing f_2. In the purpose of the vibration control of the mechanical mode, it then seems possible to keep the saturation phenomenon

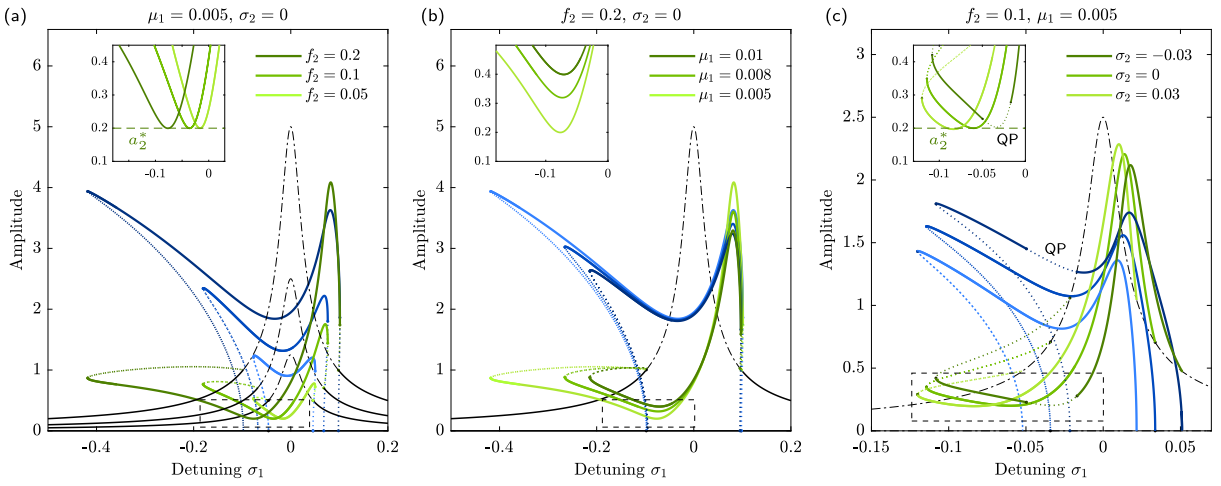

Fig. 9. Effect of variation of parameters f_2, σ_2 and μ_1 on the frequency response of the complete system (18), obtained with Manlab. (a) Variation of forcing f_2. (b) Variation of the damping μ_1. (c) Variation of the detuning σ_2 ($\omega_2 = 2\omega_1 + \sigma_2$). The common parameters are $\Lambda_1 = \Lambda_2 = \Lambda_4 = 0.1$, $\Lambda_3 = \Lambda_5 = \Lambda_6 = 0$, $\mu_2 = 0.01$, the others are specified on the plots. The uncoupled solution (a_2^U, γ_2^U) is in black and the coupled solutions (a_1^C, γ_1^C), (a_2^C, γ_2^C) are respectively in blue and green, with a darker color as the varied parameter increases. The insets show a zoom of the nonlinear antiresonance region. "QP" means quasi-periodic response.

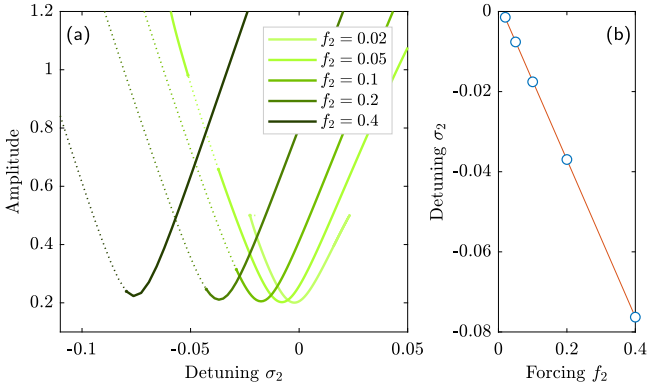

Fig. 10. (a) Amplitude of a_2^C at $\sigma_1 = 0$ as a function of the detuning σ_2 ($\omega_2 = 2\omega_1 + \sigma_2$), for several values of the forcing f_2 ($f_2 \in \{0.02; 0.05; 0.1; 0.2; 0.4\}$), obtained with Manlab with the complete system (18); (b) 'o': values of σ_2 for each minima of the curves of Fig. (a), as a function of f_2, and '—': linear fit. The parameters are: $\Lambda_1 = \Lambda_2 = \Lambda_4 = 0.1$, $\Lambda_3 = \Lambda_5 = \Lambda_6 = 0$, $\mu_1 = 0.005$, $\mu_2 = 0.01$.

of a_2^C at a fixed frequency, by adjusting the eigenmode detuning σ_2 ($\omega_2 = 2\omega_1 + \sigma_2$) as a function of f_2, in order to counterbalance the detuning of the antiresonance as a function of f_2.

To investigate this idea, Fig. 10(a) shows the amplitude a_2^C at the mechanical mode resonance $\sigma_1 = 0$ ($\bar{\Omega} = \omega_1$) as a function of the eigenmode detuning σ_2, for several values of the forcing f_2, all the other parameters being chosen constant. This was numerically obtained with Manlab, by performing a continuation in σ_2, with $\sigma_1 = 0$ and f_2 constant. This plot shows that the $a_2^C = f(\sigma_2)$ curves show a minimum, which corresponds to the value σ_2^* of σ_2 necessary to place the antiresonance of a_2^C exactly at the resonance $\sigma_1 = 0 \Leftrightarrow \bar{\Omega} = \omega_2$. Then, Fig. 10(b) shows those optimal values σ_2^* as a function of the forcing f_2. A linear fit is also plotted, showing that a linear relation

$$\sigma_2^* = -\alpha f_2, \quad \alpha \in \mathbb{R}^+, \tag{42}$$

is at hand. The slope is negative, in agreement with that can be observed in Figs. 9(a, c), in which one has to reduce the detuning σ_2 to shift the antiresonance to the high frequencies to counterbalance an increase of f_2.

The $\sigma_2^* = -\alpha f_2$ curve of Fig. 11(b) has been tested, to verify that the antiresonance of a_2^C can be placed at the resonance frequency ω_2 regardless of the excitation level. Several resonance curves for different excitation levels f_2 are shown in Fig. 11(a), with, for each response, the value of the detuning σ_2 adjusted to verify Eq. (42). One can observe in the inset that the antiresonance frequency is perfectly kept at $\sigma_1 = 0$, allowing for a perfect autotuning. Then, using Manlab, we performed a continuation with f_2 left free, $\sigma_1 = 0$ and σ_2 function of f_2 with Eq. (42). We obtained Fig. 11(b), that shows that using the autotuning relation (42) enables to recover the saturation phenomenon, since the amplitude $a_2^C(\sigma_1 = 0)$ at the antiresonance is independent of f_2. Fig. 11(b) also

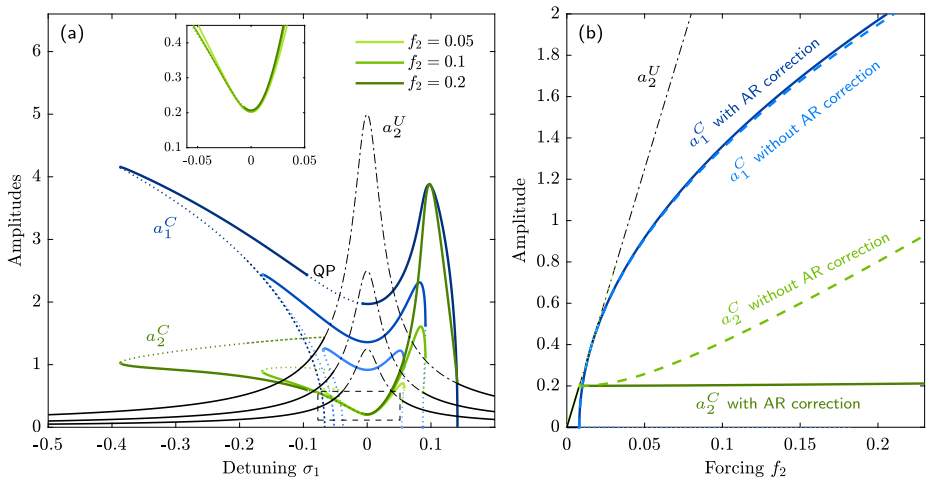

Fig. 11. Typical response of the complete system (18) obtained with Manlab, with the value of the detuning σ_2 adjusted as a function of the forcing f_2 according to Fig. 10(b) to place the nonlinear antiresonance (AR correction) at $\sigma_1 = 0$. (a) frequency response: amplitudes a_1 and a_2 as a function of the detuning σ_1 for several values of the forcing f_2 ($f_2 \in \{0.05; 0.1; 0.2\}$), with a darker color as f_2 increases. The inset shows a zoom of the nonlinear antiresonance region. "QP" means quasi-periodic response; (b) Force response: amplitudes a_1 and a_2 at $\sigma_1 = 0$ as a function of the forcing f_2 with ('—') and without ('- -') the AR correction. The parameters are: $\Lambda_1 = \Lambda_2 = \Lambda_4 = 0.1$, $\Lambda_3 = \Lambda_5 = \Lambda_6 = 0$, $\mu_1 = 0.005$, $\mu_2 = 0.01$.

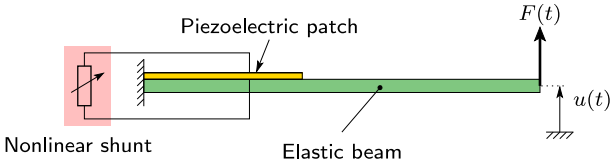

Fig. 12. Beam with a piezoelectric patch and a nonlinear shunt.

shows the response of the system without the autotuning (with $\sigma_2 = 0$), showing that the saturation phenomenon is lost but that a vibration reduction at the resonance of a_2 is however achieved, since the green dashed curved (a_2^C without AR correction) is below the black dash-dotted curve (a_2^U). One can also observe that the amplitude of the electrical mode a_1^C is almost left unchanged, at the antiresonance, by the non-zero value of Λ_1, since the two blue solid and dashed curves are almost merged.

4.4. Conclusions

The comparison between the responses of the complete system (18) and the MS analytical solution (27) of the simplified system (without the non-resonant terms) seen in the previous sections leads to the following conclusions, regarding the design of the vibration absorber. We studied only the effect of the leading resonant-term, of coefficient Λ_1. The complete system (18) shows a more complicated frequency response in comparison to that of the simplified one, due to the non-resonant term, that appeared to have a significant effect on the response. First, a kind of softening behavior is observed, since the curves show an overall bending to the low frequencies. It is responsible of a shift of the antiresonance frequency of the mechanical mode, that is now a function of the forcing and the damping. Secondly, we showed that the amplitude of this antiresonance remains independent of the forcing amplitude, with a phase γ_1^C also locked at $3\pi/2$. Thirdly, in order to correct this antiresonance shift, we showed that it is possible to continuously adjust the frequency ω_1 of the electrical mode as a function of the forcing amplitude f_2 (with the linear relation of Eq. (42) and $\sigma_2 = \omega_2 - 2\omega_1 \Rightarrow \omega_1 = (\omega_2 + \alpha f_2)/2$), to keep the antiresonance frequency independent of f_2 and then to obtain a perfect saturation phenomenon of the mechanical mode amplitude a_2^C at the antiresonance. Qualitatively, since $\alpha > 0$, one has to overtune ω_1 with respect to the perfect tuning $\omega_1 = \omega_2/2$. A last comment is that the proportionality coefficient α depends on the other parameters of the system and in particular on the nonlinearity coefficient β. This will be investigated in Section 5.7.

5. Application to a real structure

We investigate in the section the application of the proposed nonlinear shunt absorber to an arbitrary elastic structure with piezoelectric patches (as depicted in Fig. 1) and we give an example considering a beam structure (Fig. 12).

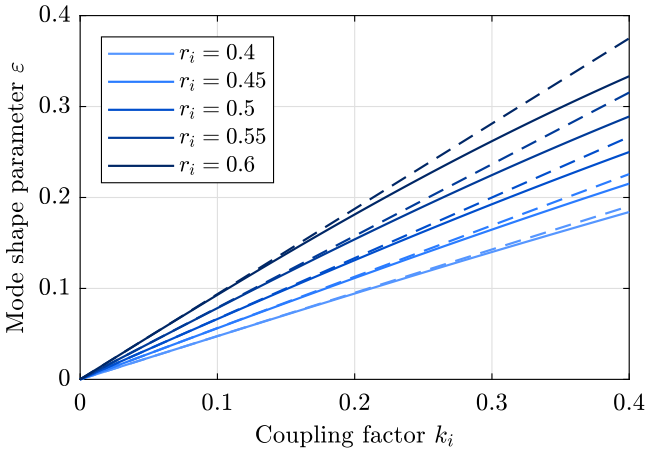

Fig. 13. Mode shape parameter ε as a function of the electromechanical coupling factor k_i for different values of the frequency ratio r_i, as specified. '—': exact value from Eq. (14); '- -': linear approximation, Eq. (46).

5.1. Effect of electromechanical modal expansion

The simplified model of Section 3 aimed at raising simple design guidelines, which were extended to a more realistic model in Section 4. However, both models are valid within the electromechanical modal expansion of Eqs. (15) and (16). The effect of this latter is investigated in this section.

First, the electromechanical modal analysis of Section 2.2 shows that the two dimensionless natural frequencies of the system are ω_1 and ω_2. Analyzing Eq. (12) shows that ω_1 is slightly smaller than r_i and ω_2 is slightly above 1. This shows that the two corresponding dimensioned natural frequencies of the system, denoted $\tilde{\omega}_e = \omega_1\hat{\omega}_i$ and $\tilde{\omega}_i = \omega_2\hat{\omega}_i$, are such that $\tilde{\omega}_e \lesssim \omega_e$ and $\tilde{\omega}_i \gtrsim \hat{\omega}_i$: they are located apart from the two uncoupled frequencies ω_e and $\hat{\omega}_i$, because of the piezoelectric coupling. This means that all the frequency responses shown in Sections 3 and 4, and consequently the frequency band of vibration reduction, are *in the vicinity of the $\tilde{\omega}_i$ resonance*, slightly above the open circuit resonance at $\hat{\omega}_i$, obtained with $Q = 0$ in Eqs. (6). This will be illustrated in Fig. 16.

Then, following the modal expansion (4), the displacement of the point of the structure can be written $\boldsymbol{u}(t) = \boldsymbol{\Phi}_i q_i(t) = \boldsymbol{\Phi}_i \bar{q}_i(t)/\sqrt{m_i}$, where the scaling of Eq. (9) has been used. We consider that the external forcing is harmonic, of angular frequency Ω. Then, the first order solutions for the displacement and charge electromechanical modal coordinates $(x_1(t), x_2(t))$ seen in Sections 3 and 4, Eqs. (26)a,b, and the electromechanical modal change of variables (16)a enable writing the displacement as:

$$\boldsymbol{u}(t) = \frac{\boldsymbol{\Phi}_i}{\sqrt{m_i}}\Big[\underbrace{-\varepsilon\, a_1 \cos\left(\frac{\Omega}{2}t - \frac{\gamma_1+\gamma_2}{2}\right)}_{x_1(t)} + \underbrace{a_2\cos\left(\Omega t - \gamma_2\right)}_{x_2(t)}\Big], \tag{43}$$

As a first result, because the leading harmonics of $x_1(t)$ is $\Omega/2$ (H1/2) and the one of $x_2(t)$ is Ω (H1), there is a frequency splitting between $x_1(t)$ and $x_2(t)$. Consequently, the *saturation phenomenon* (see Fig. 11) that has been exhibited on $x_2(t)$ in Sections 3 and 4 is equally *observed on the mechanical displacement* $\boldsymbol{u}(t)$ of any point of the structure, at the driving frequency Ω. In addition, the electromechanical modal change of variables (16)a creates a subharmonic component (H1/2) in $\boldsymbol{u}(t)$, proportional to $x_1(t)$, a priori of a smaller amplitude because of the ε factor.

In the same manner, Eqs. (9), (16)b give, for the electrical charge:

$$Q(t) = \frac{1}{\sqrt{L}}\Big[\underbrace{a_1\cos\left(\frac{\Omega}{2}t - \frac{\gamma_1+\gamma_2}{2}\right)}_{x_1(t)} + \varepsilon\,\underbrace{a_2\cos\left(\Omega t - \gamma_2\right)}_{x_2(t)}\Big]. \tag{44}$$

Here, the leading harmonics is H1/2, with a H1 harmonics of smaller amplitude, because of the ε factor.

5.2. Saturation amplitude and design

To evaluate the relevant parameters for the design of the nonlinear shunt, we base ourselves on the amplitude a_2^* of the mechanical mode saturation given by Eq. (34). Inserting this equation into Eq. (43), the Ω (H1) harmonics amplitude of the displacement vector then reads:

$$\boldsymbol{u}^*_{\mathrm{H1}} = \frac{a_2^*\boldsymbol{\Phi}_i}{\sqrt{m_i}} = u^*_{\mathrm{H1}}\boldsymbol{\Phi}_i, \quad \text{with} \quad u^*_{\mathrm{H1}} = \frac{2\omega_2\mu_1}{\Lambda_2\sqrt{m_i}} \tag{45}$$

Table 1
Typical values of capacitance C_{pi} and β_1/β_2 for a thickness/length ratio $h_p/l_p = 0.01$, a frequency ratio $r_i = 0.5$, a typical dielectric permittivity $\epsilon_{33} = 2000\epsilon_0 \simeq 2 \cdot 10^{-8}$ F/m ($\epsilon_0 = 8.82 \cdot 10^{-12}$ F/m is the vacuum permittivity) for a PZT like piezoelectric material [58], as a function of width b.

b_p [m]	1e−6	1e−3	1e−2	1e−1
C_{pi}	2 pF	2 nF	20 nF	200 nF
$\beta_1/\beta_2 = 1/(C_{pi}^2 r_i^2)$	10^{24}	10^{18}	10^{16}	10^{14}

We can verify that the above amplitude is logically independent of the scaling of the mode shape $\boldsymbol{\Phi}_i$ since the modal mass is $m_i = \boldsymbol{\Phi}_i^{\mathrm{T}} \boldsymbol{M} \boldsymbol{\Phi}_i$ (see Eqs. (5)).

To go further, we consider practical values of the parameters. As explained in Section 2.2, the parameter ε is small and depends on the electromechanical coupling factor k_i and the tuning of the electrical resonance r_i. To easily analyze the mathematical results, we neglect in Δ the term $4r_i^2 k_i^2$ and Eqs. (14) and (12) give:

$$\varepsilon \simeq \frac{k_i r_i}{1 - r_i^2}, \quad \omega_2 \simeq 1. \tag{46}$$

Fig. 13 shows that the above linear approximation of ε as a function of k_i is valid on a large range of k_i values, below $k_i = 0.2$. Then, because ε is small, we approximate μ_1 and μ_2 in Eq. (19) by:

$$\mu_1 \simeq \xi_e r_i, \quad \mu_2 \simeq \xi_i. \tag{47}$$

Finally, $\boldsymbol{u}_{\mathrm{H1}}$ depends on Λ_2, which depends on the choice of the nonlinear shunt in Eq. (2).

Considering the first case of nonlinear shunt for which the voltage is proportional to the squared electrical charge (Eq. (2)a)), one obtains, with Eqs. (21) and (23), $\Lambda_2 = 2\varepsilon\beta_1 r_i^3 \hat{\omega}_i C_{\mathrm{p}i}^{3/2}$, which gives:

$$\boldsymbol{u}_{\mathrm{H1}}^{*(1)} = \frac{\xi_e}{k_i \beta_1} \frac{1 - r_i^2}{r_i^3 C_{\mathrm{p}i}^{3/2}} \frac{\boldsymbol{\Phi}_i}{\hat{\omega}_i \sqrt{m_i}} \tag{48}$$

In the second case for which the voltage is proportional to the squared piezoelectric voltage (Eq. (2)b), one obtains, with Eqs. (21) and (24),

$$\Lambda_2 \simeq 2\lambda_1 \varepsilon + \lambda_2 - 2\lambda_3 \varepsilon = \frac{2r_i^2 k_i (1 - k_i^2)}{1 - r_i^2} \frac{\beta_2 \hat{\omega}_i}{\sqrt{C_{\mathrm{p}i}}},$$

which gives, with $1 - k_i^2 \simeq 1$:

$$\boldsymbol{u}_{\mathrm{H1}}^{*(2)} = \frac{\xi_e}{k_i \beta_2} \frac{(1 - r_i^2)\sqrt{C_{\mathrm{p}i}}}{r_i} \frac{\boldsymbol{\Phi}_i}{\hat{\omega}_i \sqrt{m_i}} \tag{49}$$

Eqs. (48) and (49) share similarities. If one wants to minimize the saturation vibration amplitude of the structure $\boldsymbol{u}_{\mathrm{H1}}^*$, one has to consider the factor $\eta = \xi_e/(k_i\beta)$ as low as possible, *i.e.* with a low electrical shunt damping ratio ξ_e and high piezoelectric coupling factor k_i and nonlinearity coefficient β. Since the values of ξ_e and k_i are in practice limited by the material constants of the components, one can imagine increasing β as much as possible, with a suitable electronic circuit, to efficiently improve the shunt performance, and/or balance a too high ξ_e or a two low k_i.

5.3. Order of magnitude of coefficient β

Following the previous section and considering the two choices for the nonlinear shunt design in Eq. (2), if we consider a given targeted saturation amplitude $\boldsymbol{u}_{\mathrm{H1}}^*$, the ratio between $u_{\mathrm{H1}}^{*(1)}$ and $u_{\mathrm{H1}}^{*(2)}$ gives the order of magnitude of β_1/β_2 of the two choices:

$$\frac{u_{\mathrm{H1}}^{*(1)}}{u_{\mathrm{H1}}^{*(2)}} = 1 = \frac{\beta_2}{\beta_1 C_{\mathrm{p}i}^2 r_i^2} \quad \Rightarrow \quad \frac{\beta_1}{\beta_2} = \frac{1}{C_{\mathrm{p}i}^2 r_i^2}. \tag{50}$$

Remember that the units of β_1 and β_2 are not the same. One observes that β_1/β_2 depends only on the piezoelectric patch capacitance $C_{\mathrm{p}i}$ and the frequency ratio r_i. In most practical cases, $C_{\mathrm{p}i}$ takes a very small value in Farads. This is illustrated in Table 1 in which the capacitance of a rectangular piezoelectric patch of length l_p, thickness h_p and width b_p is indicated, computed with:

$$C_{\mathrm{p}i} = \frac{\epsilon_{33} l_p b_p}{h_p}, \tag{51}$$

where ϵ_{33} is the permittivity of the material. Typically, if the patch is thin ($L/h = 100$) and of centimetric dimensions, $C_{\mathrm{p}i} \simeq 20$nF, which leads to a very large ratio β_1/β_2, of the order of 10^{16} F^2. This huge ratio can be explained because piezoelectric transducers typically exhibit small charges and high voltages. More insights on practical values of the gains β_k are investigated in the next section on a practical example, of centimetric size.

5.4. Electric charge order of magnitude

We evaluate here the effect of the design parameters on the value of the electric charge at the antiresonance. We consider its leading harmonics H1/2, which, considering Eqs. (44) and (35), (9), (20), reads:

$$Q^*_{\mathrm{H1/2}} = \frac{a^*_1}{\sqrt{L}} = \sqrt{\frac{2}{L\Lambda_4}}\sqrt{\frac{F-F^*}{\hat{\omega}_i^2\sqrt{m_i}}}. \tag{52}$$

In the above equation, $F^* = \boldsymbol{\Phi}_i^{\mathrm{T}}\boldsymbol{F}^*$ is the value of the forcing amplitude $F = \boldsymbol{\Phi}_i^{\mathrm{T}}\boldsymbol{F}$ at the nonlinear coupling threshold. Considering Eq. (34) and the scaling (9), one shows that:

$$F^* = 2\xi_i\hat{\omega}_i^2 m_i u^*_{\mathrm{H1}}. \tag{53}$$

In the same manner than in the previous sections, we consider successively the two shunt designs. For the first case (Eq. (2)a), one obtains, with Eqs. (21) and (23), $\Lambda_4 = \varepsilon\beta_1 r_i^3\hat{\omega}_i C_{\mathrm{p}i}^{3/2}$ which gives:

$$Q^{*(1)}_{\mathrm{H1/2}} = \sqrt{\frac{2(1-r_i^2)}{k_i\beta_1 r_i^2\hat{\omega}_i\sqrt{m_i C_{\mathrm{p}i}}}}\sqrt{F-F^*}, \quad F^* = \frac{2\xi_i\xi_e(1-r_i^2)\hat{\omega}_i\sqrt{m_i}}{k_i\beta_1 r_i^3 C_{\mathrm{p}i}^{3/2}}. \tag{54}$$

In the above equation, the relation (7) between L and ω_e as well as the approximation (46) for ε have been used.

For the second case (Eq. (2)b), one obtains, with Eqs. (21), (24), (46),

$$\Lambda_4 = \varepsilon(\lambda_1 - \lambda_2\varepsilon + \lambda_3\varepsilon^2) = \frac{r_i^4 k_i}{1-r_i^2}\left(1-o(k_i^2)\right)\frac{\beta_2\hat{\omega}_i}{\sqrt{C_{\mathrm{p}i}}},$$

where $o(k_i^2)$, of the order of k_i^2, will be neglected in the following. One then obtains:

$$Q^{*(2)}_{\mathrm{H1/2}} = \sqrt{\frac{2(1-r_i^2)C_{\mathrm{p}i}^{3/2}}{r_i^2 k_i\beta_2\hat{\omega}_i\sqrt{m_i}}}\sqrt{F-F^*}, \quad F^* = \frac{2\xi_i\xi_e(1-r_i^2)\hat{\omega}_i\sqrt{m_i C_{\mathrm{p}i}}}{k_i\beta_1 r_i} \tag{55}$$

As considered in the previous Section 5.3, by considering a given targeted threshold amplitude $\boldsymbol{u}^*_{\mathrm{H1}}$, the ratio between the two charge expressions in the two cases of shunt design gives:

$$\frac{Q^{*(1)}_{\mathrm{H1/2}}}{Q^{*(2)}_{\mathrm{H1/2}}} = \frac{\beta_2}{\beta_1 C_{\mathrm{p}i}^2} = r_i^2 \simeq 1/4, \tag{56}$$

where the last equality comes from Eq. (50) and $r_i \simeq 0.5$.

Two comments can be raised. The first one is that, considering a given threshold amplitude $\boldsymbol{u}^*_{\mathrm{H1}}$, the electric charge amplitudes estimated for the two shunt designs (Eq. (2)a or (2)b) are of the same order of magnitude, since the ratio is $\simeq 1/4$. Then, the other major parameter which influences the amplitude of the electric charge is the force threshold F^*: the smaller it is, the higher $Q^*_{\mathrm{H1/2}}$ is for a given excitation amplitude F. This is illustrated in Figs. 4(b) or 11(b), where decreasing F^* (or f_2^*) would translate the a_1^C curve to the left and thus increase the value of its amplitude for a given forcing f_2. Finally, another important parameter is $k_i\beta$ which appears in the denominator of $Q^*_{\mathrm{H1/2}}$ and in F^*. We can write $Q^*_{\mathrm{H1/2}} = \sqrt{(ax-b)/x^2}$ with $x = k_i\beta$ and a, b functions of the other parameters. One can remark that this function is increasing as a function of x, showing that *an increase of $k_i\beta$ also leads to an increase of the electric charge*. This was already observed in Figs. 5(b) and 6(a) where a_1^C increases as a function of Λ_2 and Λ_4, both proportional to $k_i\beta$.

5.5. Subharmonic of the displacement

As shown in Eq. (43), the electromechanical coupling is responsible of a parasitic subharmonic H1/2 in the displacement $\boldsymbol{u}(t)$. To estimate its relative amplitude, we compute the ratio of harmonics H1/2 and H1 at the antiresonance:

$$\frac{u^*_{\mathrm{H1/2}}}{u^*_{\mathrm{H1}}} = \frac{\varepsilon a^*_1}{a^*_2} = \varepsilon\sqrt{\frac{2(F-F^*)}{\Lambda_4\hat{\omega}_i^2\sqrt{m_i}}\frac{\Lambda_2^2}{4\omega_2^2\mu_1^2}}. \tag{57}$$

With the same reasoning as in the previous sections, for the first case of $V_{\mathrm{nl}} = \beta_1 Q^2$, one obtains $\Lambda_4 = \Lambda_2/2$ and:

$$\frac{u^{*(1)}_{\mathrm{H1/2}}}{u^{*(1)}_{\mathrm{H1}}} = \sqrt{\frac{k_i^3\beta_1}{\xi_e^2}\frac{2r_i^4 C_{\mathrm{p}i}^{3/2}(F-F^*)}{(1-r_i^2)^3\hat{\omega}_i\sqrt{m_i}}}. \tag{58}$$

For the second case of $V_{\mathrm{nl}} = \beta_2 V^2$, $\Lambda_4 = r_i^2\Lambda_2/2$ and:

$$\frac{u^{*(2)}_{\mathrm{H1/2}}}{u^{*(2)}_{\mathrm{H1}}} = \sqrt{\frac{k_i^3\beta_2}{\xi_e^2}\frac{2(F-F^*)}{(1-r_i^2)^3\hat{\omega}_i\sqrt{m_i C_{\mathrm{p}i}}}}. \tag{59}$$

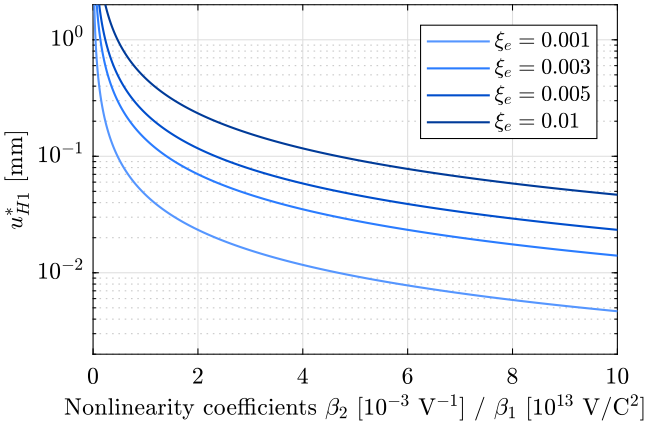

Fig. 14. Saturation amplitude $u^{*(k)}_{\mathrm{H1}}$, $k = 1, 2$ as a function of β_k, from Eqs. (61) and (62), for various values of the electrical damping ratio ξ_e, as specified. The plot is related to the first mode of a beam ($\zeta_i = \zeta_1 = 1.875$) in steel ($E = 200$ GPa), with a thickness/length ratio $h/L = 0.01$, a frequency ratio $r_i = 0.5$, a dielectric permittivity $\epsilon_{33} = 2000\epsilon_0 \simeq 2 \cdot 10^{-8}$F/m ($\epsilon_0 = 8.82 \cdot 10^{-12}$F/m is the vacuum permittivity) and a coupling factor $k_i = 0.2$. In the first case, $k = 1$, the beam thickness is $b = 10$ mm.

Considering the above result, two conclusions can be drawn. First, since the subharmonic is proportional to a^*_1 (similarly to the electric charge $Q^*_{\mathrm{H1}/2}$), it is also proportional to the factor $\sqrt{F - F^*}$. Secondly, it is proportional to the factor $\sqrt{k_i^3 \beta / \xi_e^2}$, a fact that will be analyzed in Section 6.

5.6. An arbitrary thin piezoelectric beam

All the previous investigations can be applied to an arbitrary structure. To precise the design, we particularize the geometry and we consider a beam with a piezoelectric patch, as depicted in Fig. 12. To obtain the order of magnitude of the several parameters, we neglect the mechanical inertia and stiffness of the piezoelectric patch and consider in the model only those of the elastic layer (see for instance [58,70] for more refined models). We denote by (E, ρ) the Young's modulus and density of the elastic layer and we consider a rectangular cross section of width b and thickness h. l is the length of the beam. An analytical model is thus at hand and gives, for this beam (with a classical Euler–Bernoulli kinematics [71]):

$$\breve{\omega}_i \simeq \hat{\omega}_i = \frac{\zeta_i^2 h}{l^2}\sqrt{\frac{E}{12\rho}}, \quad m_i = \rho b h l/4, \quad \boldsymbol{\Phi}_i(l) = 1, \tag{60}$$

with $\zeta_1 = 1.875$, $\zeta_2 = 4.694$, $\zeta_3 = 7.855\ldots$ and $\boldsymbol{\Phi}_i(l)$ the value of the ith mode shape at the tip of the beam. To obtain a consistent order of magnitude of the electric capacitance of the piezoelectric patch, we use Eq. (51), by considering a piezoelectric patch of equivalent size to that of the elastic layer.

Introducing the above parameters in Eqs. (48) and (49) leads to:

$$u^{*(1)}_{\mathrm{H1}} = \frac{4\sqrt{3}\xi_e}{k_i \zeta_i^2 \sqrt{E}} \frac{1 - r_i^2}{r_i^3} \frac{1}{\beta_1 \epsilon_{33}^{3/2} b^2}, \tag{61}$$

$$u^{*(2)}_{\mathrm{H1}} = \frac{4\sqrt{3}\xi_e}{k_i \zeta_i^2 \sqrt{E}} \frac{1 - r_i^2}{r_i} \frac{\sqrt{\epsilon_{33}} L^2}{\beta_2 h^2}, \tag{62}$$

where $u^{*(k)}_{\mathrm{H1}}$, $k = 1, 2$, are the beam tip displacement amplitudes for the two shunt design choices. One observes that those two equations are independent of the density of the material ρ. They are composed of three factors. The first one is common two both equations; the second one depends on the piezoelectric shunt tuning $r_i = \omega_e / \hat{\omega}_i \simeq 0.5$. The third one differs in the two equations, because of the different physical nature of β_1 (of unit V/C^2) and β_2 (of units V^{-1}), stemming from the two choices for the nonlinear shunt.

In the case of the second choice ($V_{nl} = \beta_2 V_p^2$), Eq. (62) shows that the saturation value $u^{*(2)}_{\mathrm{H1}}$ of the tip amplitude of the beam, expressed in [m], does not depend on the size of the structure but only of its slenderness ratio h/l. On the contrary, $u^{*(1)}_{\mathrm{H1}}$ for the first choice ($V_{nl} = \beta_1 Q^2$) is inversely proportional to the squared size of the structure, through its squared width b^2. The dependence on the other parameters is the same for both cases. To set the ideas of the order of magnitude of β_1 or β_2 in a practical case, Fig. 14 gives the saturation amplitude $u^{*(k)}_{\mathrm{H1}}$ of the beam's tip as a function of β_k. In the case of a centimetric thin beam ($h/l = 0.01$) in steel, with a PZT piezoelectric patch, a saturation amplitude of 0.05 mm is obtained for $\beta_2 \simeq 0.005$ V^{-1}, whereas $\beta_1 \simeq 5 \cdot 10^{13}$ V/C^2, in agreement with Table 1. In a practical case, since analog nonlinear capacitors with the required level of nonlinearity are scarce in common electronic components, one would probably rely on analog multipliers or a synthetic digital shunt to realize the electronics. In those cases, huge values of β_1, naturally explained by the small electric charge generated by the piezoelectric transducers, would probably

Table 2
Parameters of the first mode of the beam used for the frequency response of Fig. 16.

$\hat{\omega}_1/(2\pi)$	ξ_1	m_1	C_{p1}	θ_1	k_1	$\Phi_1(l)$
37.51 Hz	0.005	8.9 g	32.45 nF	0.88 mN/V	0.22	1

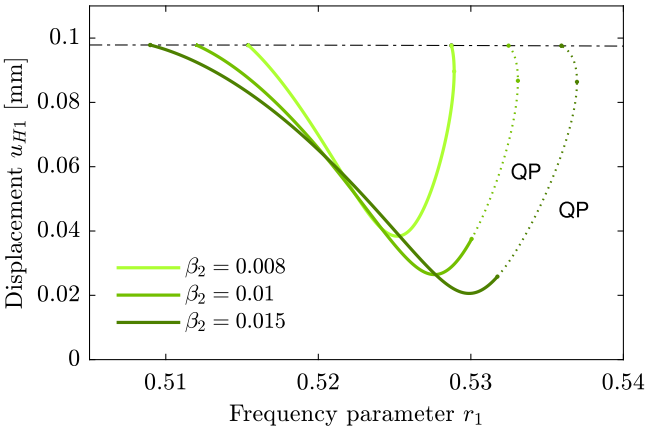

Fig. 15. Amplitude u_{H1} at the open circuit natural frequency $\Omega = \hat{\omega}_1$ of the beam tip of the beam as a function of the frequency parameter $r_1 = \omega_e/\hat{\omega}_1$, for several values of the nonlinearity coefficient β_2 ($\beta_2 \in \{0.008; 0.01; 0.015\}$ V^{-1}), as specified, and for a given value of the forcing $F = 0.53$ mN. Those curves were obtained by numerical continuation of Eqs. (6) with Manlab. The parameters are those of Table 2 and the electrical damping ratio is $\xi_e = 0.0053$.

be realized in practice using dedicated charge amplifiers, with possible complex electronic implementations. On the contrary, the second design choice of $V_{nl} = \beta_2 V_p^2$ appears more straightforward, with smaller values of β_2, and would probably lead to simpler electronic circuit designs, which motivates the practical example of the next section.

5.7. A practical example

In this section, we give an example of design of the nonlinear piezoelectric shunt on a particular structure. We choose the piezoelectric beam already used in [59]. It is a stainless steel cantilever beam (with a length of 178.8 mm, a width of 30.5 mm and a thickness of 1.1 mm) with two Physik Instrumente PIC 151 piezoelectric patches (with a length of 70 mm each, 0.5 mm thick and with wrapped electrodes) bonded on each side of the beam and electrically connected in series. An experimental modal analysis gave us the modal parameters of Table 2, for the first mode of the beam ($i = 1$). In the following, we consider that the beam is driven at its tip, with a point force $F(t) = F\cos\Omega t$.

We choose to design a shunt based on the second possible case, namely with $V_{\mathrm{nl}} = \beta_2 V^2$. Looking at Fig. 1 shows that three parameters have to be chosen to design the shunt: its inductance L, resistance R and nonlinearity coefficient β_2. The inductance L influences the electrical frequency ω_e (Eq. (7)), that has to be tuned properly to obtain the 2:1 internal resonance. In theory, it is obtained with $\omega_2/\omega_1 = \tilde{\omega}_i/\tilde{\omega}_e = 0.5$. Following Fig. 2, ω_e has to be overtuned with respect to $\hat{\omega}_i/2$ and with the present electromechanical coupling factor of $k_i = 0.22$, an estimation of the tuning is $r_i \simeq 0.525$.

Moreover, to lock the antiresonance at a given frequency, this tuning slightly depends on the amplitude of the motion and other parameters, as explained in Section 4. We then use a numerical continuation of the modal reduced order model (6) as a function of the electrical frequency ω_e to precisely determine it. It is obtained in practice with Manlab, by leaving ω_e free whereas the driving frequency Ω and forcing F are prescribed. Since we are targeting an antiresonance in the middle of the frequency band of vibration reduction, we choose here $\Omega = \tilde{\omega}_i$: the resonance of the coupled electromechanical system, corresponding to $\bar{\Omega} = \omega_2$ or $\sigma_1 = 0$ in Sections 3 and 4. As explained in Section 5.1, $\tilde{\omega}_i$ is slightly above the open circuit resonance of the system at $\Omega \simeq \hat{\omega}_i$. With Eq. (12), it is clear that $\tilde{\omega}_i = \omega_2\hat{\omega}_i$ depends on k_i and r_i. Consequently, we choose our initial guess $r_i = 0.525$, which leads to $\tilde{\omega}_1 = 37.85$ Hz with Eq. (12).

Fig. 15 (analogous to Fig. 10(a) in the case of the modal model Eqs. (18)) is obtained. It shows that the amplitude $u^{(2)}_{\mathrm{H1}}$ of the first harmonics of the beam tip has a minimum for a certain value r_i^* of the frequency ratio r_i that correspond to place the antiresonance of $u^{(2)}_{\mathrm{H1}} = f(\Omega)$ exactly at $\Omega = \tilde{\omega}_1$. This plot is also valuable since it enables to visualize the value of β_2 necessary to obtain a certain amplitude threshold $u^{*(2)}_{\mathrm{H1}}$. For instance, the dark green curve shows that $\beta_2 = 0.015$ V^{-1} leads to an amplitude threshold of $u^{*(2)}_{\mathrm{H1}} = 0.02$ mm and that a tuning $r_i = 0.5309$ is necessary for the AR correction at this forcing ($F = 0.53$ mN). The obtained tunings for the three values of β_2 shown in Fig. 15 are, as expected, slightly above our initial guess of $r_i = 0.525$.

Using the values of r_i^* taken from Fig. 15, Fig. 16 shows the frequency response of the first harmonics of the beam tip $u^{(2)}_{\mathrm{H1}} = f(\Omega)$ and the subharmonics of the electric charge $Q_{\mathrm{H1/2}} = f(\Omega)$. Instead of plotting this frequency response for several values of the forcing F, which would give a plot similar to Fig. 11, we show here the frequency response for several values of the nonlinearity coefficient β_2 for a given value of the external forcing F. This plot confirms that the AR correction obtained by adjusting r_i according to the

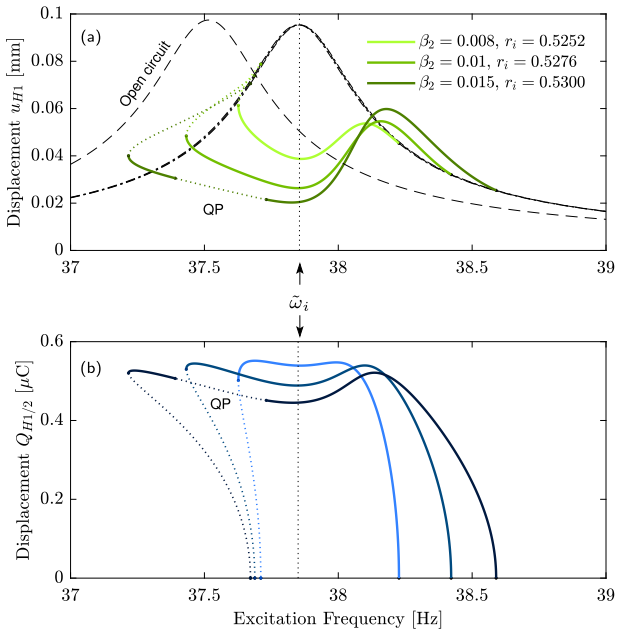

Fig. 16. Resonant response around the first resonance of the beam for several values of the nonlinearity coefficient β_2 ($\beta_2 \in \{0.008; 0.01; 0.015\}$ V^{-1}) and the nonlinear shunt tuned to obtain the nonlinear antiresonance at $\Omega = \hat{\omega}_1$, according to the minima of the curves in Fig. 15 ($r_1 = \omega_e/\hat{\omega}_1 \in \{0.5252; 0.5276; 0.5300\}$). (a) amplitude of the first harmonics of the beam's tip displacement u_{H1} and (b) amplitude of the subharmonic of the electrical charge $Q_{H1/2}$ obtained by numerical continuation of Eqs. (6) with Manlab, with a darker blue as β_2 increases. The parameters are those of Table 2, with $F = 0.53$ mN and $\xi_e = 0.0053$.

minima of Fig. 15 works since the nonlinear antiresonance is perfectly located at $\Omega = \tilde{\omega}_1$, the resonance of the coupled system. This plot also shows the linear resonances of the system, in the vicinity of $\Omega = \tilde{\omega}_i \simeq 37.85$ Hz. The slight dependence of $\Omega = \tilde{\omega}_i$ upon r_i is also visible in Fig. 16(a), since three linear resonances are obtained in dashed–dotted lines. The open circuit resonance around $\hat{\omega}_i = 37.51$ Hz is also shown in dashed lines. An interesting point is that increasing the value of β_2 slightly decreases the value of the electrical charge in Fig. 16(b).

Moreover, as already observed in Section 4, some quasiperiodic (QP) responses are obtained in Fig. 16. They can be close to the antiresonance point and seems to approach it as β_2 or F are increased. Those QP responses are also obtained in Fig. 15. Some examples of QP response as a function of time are shown in Figs. 17(d, e). There amplitude is of the same order of magnitude than the one of the periodic response at the antiresonance point (Figs. 17(b, c)), leading to think that this QP responses are not an issue for the vibration reduction. On the contrary, it can be observed that there is a unexpected strong effect of the subharmonic H1/2 on the total response in displacement, since its amplitude is of the same order of magnitude than the leading harmonics H1. This is the joint consequence of the large coupling factor $k_1 = 0.22$ used in the simulations as well as the fact that at the antiresonance point, the H1 harmonics is small because of the saturation phenomenon, leading to H1/2 harmonics of the same order of magnitude.

6. Design guidelines and parameter optimization for high vibration attenuation

As highlighted in the previous section, the design parameters that have to be chosen and controlled in a given application of the nonlinear shunt are the electrical frequency tuning $r_i = \omega_e/\hat{\omega}_i$, the nonlinearity coefficient β, the electrical damping factor ξ_e and the piezoelectric coupling factor k_i. Here is a set of guidelines that can be considered when selecting each parameter.

Firstly, one has to remark that the response of the nonlinear shunt is amplitude dependent, as shown for instance in Fig. 11. It means that, contrary to a fully linear system, the shape of the frequency response depends on the amplitude F of the forcing. On the contrary, the major property of the shunt is the saturation phenomenon, that depends on the vibration amplitude threshold u^*_{H1}, which is the minimum vibration amplitude above which it is independent of the forcing. This occurs at a particular driving frequency, close to twice the electrical frequency ω_e, that has to be tuned close to half the targeted resonance, such that $r_i = \omega_e/\hat{\omega}_i \simeq 0.5$ in order to activate the energy transfer thanks to the 2:1 internal resonance.

The main design criterion is thus the amplitude threshold u^*_{H1}, that we want to be as small as possible. In addition, the amplitude of the electric charge $Q^*_{H1/2}$ during the energy transfer has also to be considered for the design of the electrical components of the circuit. Finally, the electromechanical coupling creates a subharmonic H1/2 in the displacement signal that can have a non negligible amplitude with respect to the H1 harmonics, and thus decreases the damping performance (see Fig. 17). The harmonics ratio $u^*_{H1/2}/u^*_{H1}$, to be minimized, is thus also a design criterion.

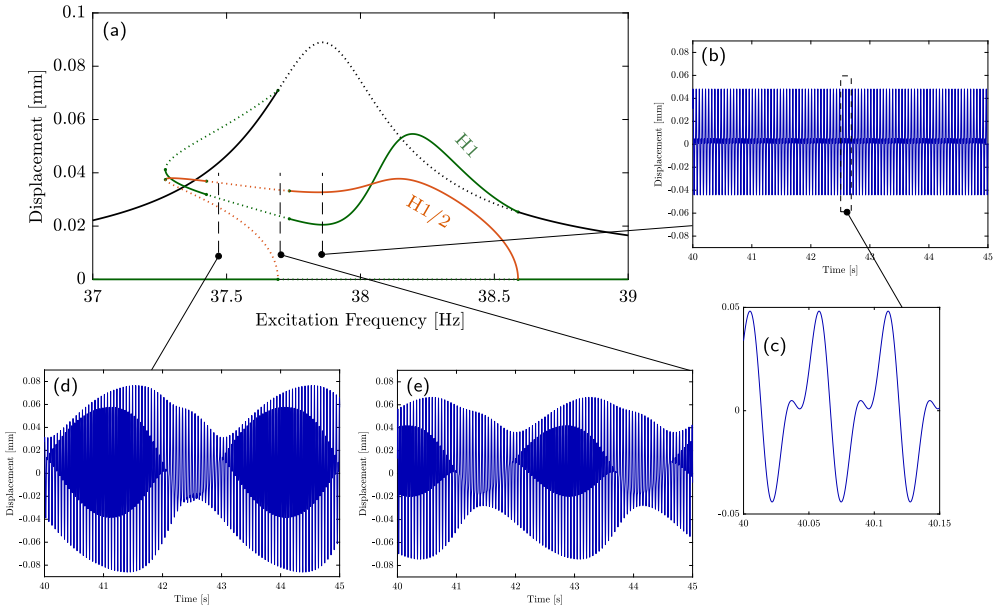

Fig. 17. (a) Resonant response around the first resonance of the beam with both the leading harmonics H1 and the subharmonic H1/2 of the beam's tip displacement (same case as Fig. 15 for $\beta_2 = 0.015\ \mathrm{V}^{-1}$); (b, c): periodic response at the antiresonance point; (d, e): examples of quasi-periodic responses, obtained by time integration. The parameters are those of Table 2, with $F = 0.53$ mN and $\xi_e = 0.0053$.

As shown in Sections 5.2 and 5.5:

$$u^*_{\mathrm{H1}} \propto \frac{\xi_e}{k_i\beta} = \eta, \quad \frac{u^*_{\mathrm{H1/2}}}{u^*_{\mathrm{H1}}} \propto \sqrt{\frac{k_i^3\beta}{\xi_e^2}} = \frac{1}{\eta}\sqrt{\frac{k_i}{\beta}}, \tag{63}$$

where $\propto$ means "proportional to". Consequently, to minimize the saturation amplitude u^*_{H1}, one has to choose η as small as possible. However, decreasing η leads to an increase of the subharmonic $u^*_{\mathrm{H1/2}}$... Considering the criterion "minimize u^*_{H1} *and* $u^*_{\mathrm{H1/2}}$", one can first choose the *electrical damping factor* ξ_e *as small as possible*. It is linked to the electrical resistance of the electronic circuit built for the shunt. Decreasing it is often limited in practice by the inherent resistance of the wires. Using an active negative capacitance synthetic circuit could be an alternative to artificially decrease ξ_e (see *e.g.* [4]). Then, one can remark that the piezoelectric coupling factor k_i and the nonlinearity parameter β play the same role and that their product $k_i\beta$ has to be as large as possible to minimize η and thus u^*_{H1}. On the contrary, the subharmonic amplitude $u^*_{\mathrm{H1/2}}$ is directly linked to the piezoelectric coupling. Then, a correct design should be with *a low (but non-zero) piezoelectric coupling factor* k_i to minimize $u^*_{\mathrm{H1/2}}$, which can be counterbalanced by *a high nonlinearity coefficient* β. In particular, if a given u^*_{H1} is targeted, one can think of minimizing $u^*_{\mathrm{H1/2}}$ by decreasing k_i while increasing β in the same proportion, to keep $k_i\beta$ (and u^*_{H1}) constant.

In most applications (linear shunt damping, energy harvesting), the piezoelectric coupling factor k_i has to be as high as possible, which also leads to a good performance here by minimizing the saturation amplitude u^*_{H1}. This is achieved by selecting a quality piezoelectric material as well as with suitable optimization of the geometry and placement of the piezoelectric patch on the structure (see [70,72]). It can be also improved by adding a negative capacitance in the shunt circuit, since it is equivalent to artificially increase the coupling factor [59]. On the contrary, for our present application, a not too high k_i is preferable to minimize the subharmonic amplitude, and the opposite reasoning has to be followed, allowing piezoelectric materials with lower coupling constants and non optimal geometry/placement of the patches.

As shown in Section 5.4, the amplitude $Q^*_{\mathrm{H1/2}}$ of the electric charge is an increasing function of $k_i\beta$. It is also proportional to $\sqrt{F - F^*}$, with F^* being proportional to u^*_{H1} (see Eq. (53)). It then means that optimizing the parameters to decrease u^*_{H1} also leads to an increase of $Q^*_{\mathrm{H1/2}}$. Moreover, increasing $k_i\beta$ or decreasing ξ_e has also the negative effect to widen the bistability region of the response curve in which a potential high amplitude response of the system can be reached, on the sides of the antiresonance (see Fig. 5, since Λ_2 is proportional $k_i\beta$ and μ_1 is proportional to ξ_e). Consequently, the benefit gained by decreasing the amplitude threshold u^*_{H1} has a direct effect on increasing the electrical charge in the circuit and widening the side bistable regions.

In addition, the parameter r_i must be chosen so that the coupled solution appears and must be slightly corrected as a function of the values of β and F, as illustrated in Sections 4.3 and 5.7. It has been shown in Fig. 10 that the correct tuning r_i^* is a linear function of the forcing F, with a coefficient that depends on the other parameters. Consequently, a performant shunt design should include a tuning correction of the electrical mode, using the proportionality relation (42). In practice, since the antiresonance occurs for a phase locking $\gamma_1 = 3\pi/2$, this property could be used to estimate the α proportionality coefficient.

7. Conclusion

In this paper, a passive nonlinear vibration absorber has been designed by utilizing a nonlinear piezoelectric electric shunt circuit with quadratic non-linearity. The quadratic non-linearity has been chosen to create a 2:1 internal resonance between a given resonant (mechanical) mode of the primary structure and a resonant electric circuit tuned at the order two subharmonic. The main feature to exploit from the 2:1 internal resonance is the saturation phenomenon, which leaves the mechanical amplitude independent of the forcing amplitude above a threshold. It is linked to a nonlinear energy transfer from the mechanical mode to the electric mode, leading to an efficient vibration attenuation near the resonance frequency.

Since the coupling of the mechanical mode and the electric mode through the piezoelectric patch breaks the invariance of those linear modes, the $2:1$ internal resonance properties are directly linked to the electromechanical modal coordinates, that are linear combination of the electrical and mechanical modes. However, because the energy is transferred from the excitation frequency harmonic to the subharmonic, we proved that this does not break the pure saturation phenomenon that is created on the mechanical amplitude of the structure at the driving frequency. However, this invariance break is also responsible of an unwanted subharmonic component in the displacement.

The choice of the nonlinear shunt parameters (piezoelectric coupling factor k_i, inductance L, resistance R and nonlinearity parameter β) has also been thoroughly addressed. It was shown that improving the performance of the shunt, by lowering as much as possible the mechanical amplitude coupling threshold u^*_{H1}, relies on decreasing as much as possible the factor $\eta = \xi_e/(k_i\beta)$, with ξ_e the dimensionless damping ratio proportional to R. Consequently, the electric circuit of the shunt must be designed as less resistive as possible, and, contrary to more classical shunt applications, the piezoelectric coupling factor k_i must be chosen not so high to minimize the subharmonic component creation. The main design parameter is thus the nonlinearity parameter β, that has to be chosen as high as possible.

The second design parameter set is the electrical tuning of the shunt, linked to the inductance L. The electrical frequency ω_e has to be chosen close to half the short circuit natural frequency of the targeted mechanical mode: $\omega_e \simeq \hat{\omega}_i/2$ to activate the $2:1$ internal resonance. The fine tuning depends on the piezoelectric coupling factor k_i (because of the invariance break considered above) in a constant fashion, but also slightly on the forcing amplitude. This unexpected effect is directly related to the high value of the non resonant term of coefficient Λ_1 in the electromechanical modal system. This high value of Λ_1 cannot be avoided with the architecture of our shunt. However, it was proven that the relation between the fine tuning of ω_e as a function of the forcing amplitude is linear, which gives a simple manner to correct this effect in a practical electronic circuit implementation.

Two shunt designs have also been tested (see Eqs. (2)). In theory, no difference of performance has been shown between both designs in the shunt performance and in the shape of the frequency response. The only notable difference is in the numerical value of the nonlinearity coefficient β, that has to be chosen very high in the first design ($V_{\mathrm{nl}} = \beta Q^2$, $\beta \simeq 5 \cdot 10^{13}\mathrm{V/C^2}$) and small for the other one ($V_{\mathrm{nl}} = \beta V^2$, $\beta \simeq 5 \cdot 10^{-3}\mathrm{V^{-1}}$). This huge difference in the orders of magnitudes has to be considered in a practical implementation of the electronic circuit. If electronic multiplier components are used like in [20], the second design has probably to be preferred.

Some quasi-periodic (QP) solutions have also been observed in our simulations, close to the antiresonance point. Those QP solutions are responsible for beatings superimposed to the classical periodic solutions, that could slightly decrease the vibration control performance, depending on the beating amplitude. The appearance of those QP responses is also probably linked to the increase of the performance factor $k_i\beta/\xi_e$, in a non trivial manner. A way of investigation should be the tracking of the Neimark–Sacker bifurcations, using numerical continuation, as proposed for instance in [73]. The study of those QP solutions is left for further studies.

Finally, one must bear in mind that this kind of nonlinear shunt is forcing amplitude dependent. The first consequence is that the amplitude reduction appears above an amplitude threshold. So, below this amplitude, a classical linear absorber (like a resonant shunt for instance [7]) has better performance. However, above the threshold, since the amplitude at the antiresonance saturates, the present nonlinear shunt behaves better and better as long as the forcing amplitude increases. It is thus well suited to cases for which the force is harmonics (like in rotating machines [74]), with a frequency in the vicinity of the mechanical resonance. In other cases of a force with a large band frequency content, the side resonance created by the non-resonant term Λ_1 on the right of the antiresonance, as seen in Fig. 11 or 16, could be an issue.

Declaration of competing interest

The authors declare that they have no known competing financial interests or personal relationships that could have appeared to influence the work reported in this paper.

Acknowledgments

The *Région Hauts de France* and the *Carnot ARTS Institute*, France are warmly thanked for the PhD grant of the first author.

References

[1] N.W. Hagood, A. Von Flotow, Damping of structural vibrations with piezoelectric materials and passive electrical networks, J. Sound Vib. 146 (2) (1991) 243–268.

[2] S. Behrens, A.J. Fleming, S.O.R. Moheimani, Electromagnetic shunt damping, in: Proceedings of the 2003 IEEE/ASME International Conference on Advanced Intelligent Mechatronics (AIM 2003), 2003, pp. 1145–1150.

[3] J.A.B. Gripp, D.A. Rade, Vibration and noise control using shunted piezoelectric transducers: A review, Mech. Syst. Signal Process. 112 (2018) 259–383.

[4] M. Auleley, O. Thomas, C. Giraud-Audine, H. Mahé, Enhancement of a dynamic vibration absorber by means of an electromagnetic shunt, J. Intell. Mater. Syst. Struct. 32 (3) (2020) 331–354, http://dx.doi.org/10.1177/1045389X20957097.

[5] S. Krenk, Frequency analysis of the tuned mass damper, J. Appl. Mech. 72 (2005) 936–942.

[6] M. Vakilinejad, A. Grolet, O. Thomas, A comparison of robustness and performance of linear and nonlinear lanchester dampers, Nonlinear Dynam. 100 (2020) 269–287, http://dx.doi.org/10.1007/s11071-020-05512-x.

[7] O. Thomas, J. Ducarne, J.-F. Deü, Performance of piezoelectric shunts for vibration reduction, Smart Mater. Struct. 21 (1) (2012) 015008, http://dx.doi.org/10.1088/0964-1726/21/1/015008.

[8] G. Caruso, A critical analysis of electric shunt circuits employed in piezoelectric passive vibration damping, Smart Mater. Struct. 10 (2001) 1059–1068.

[9] M. Berardengo, S. Manzoni, O. Thomas, M. Vanali, Piezoelectric resonant shunt enhancement by negative capacitances: Optimisation, performance and resonance cancellation, J. Intell. Mater. Syst. Struct. 29 (12) (2019) 2581–2606.

[10] R. Darleux, B. Lossouarn, J.-F. Deü, Broadband vibration damping of nonperiodic plates by piezoelectric coupling to their electrical analogues, Smart Mater. Struct. 29 (2020) 054001.

[11] G. Gatti, M. Brennan, B. Tang, Some diverse examples of exploiting the beneficial effects of geometric stiffness nonlinearity, Mech. Syst. Signal Process. 125 (2019) 4–20.

[12] D.F. Ledezma-Ramirez, P.E. Tapia-González, N. Ferguson, M.J. Brennan, B. Tang, Recent advances in shock vibration isolation: An overview and future possibilities, Appl. Mech. Rev. 71 (2019) 060802.

[13] A.F. Vakakis, O. Gendelman, Energy pumping in nonlinear mechanical oscillators: Part II - Resonance capture, J. Appl. Mech. 68 (2001) 42–48.

[14] Z. Lu, Z. Wang, Y. Zhou, X. Lu, Nonlinear dissipative devices in structural vibration control: A review, J. Sound Vib. 423 (2018) 18–49.

[15] B. Vaurigaud, A.T. Savadkoohi, C.-H. Lamarque, Targeted energy transfer with parallel nonlinear energy sinks. Part I: Design theory and numerical results, Nonlinear Dynam. 66 (2011) 763–780.

[16] S. Benacchio, A. Malher, J. Boisson, C. Touzé, Design of a magnetic vibration absorber with tunable stiffnesses, Nonlinear Dynam. 85 (2016) 893–911.

[17] V. Iurasov, P.-O. Mattei, Bistable nonlinear damper based on a buckled beam configuration, Nonlinear Dynam. 99 (2020) 1801–1822.

[18] D. Qiu, S. Seguy, M. Paredes, Design criteria for optimally tuned vibro-impact nonlinear energy sink, J. Sound Vib. 442 (2019) 497–513.

[19] B. Zhou, F. Thouverez, D. Lenoir, Essentially nonlinear piezoelectric shunt circuits applied to mistuned bladed disks, J. Sound Vib. 333 (2014) 2520–2542.

[20] T.M.P. Silva, M.A. Clementino, C.D.M. Jr., A. Erturk, An experimentally validated piezoelectric nonlinear energy sink for wideband vibration attenuation, J. Sound Vib. 437 (2018) 68–78.

[21] G. Zhao, G. Raze, A. Paknejad, A. Deraemaeker, G. Kerschen, C. Collette, Active nonlinear energy sink using force feedback under transient regime, Nonlinear Dynam. 102 (2020) 1319–1336.

[22] G. Habib, T. Detroux, R. Viguié, G. Kerschen, Nonlinear generalization of Den Hartog's equal-peak method, Mech. Syst. Signal Process. 52–53 (2015) 17–28.

[23] G. Raze, G. Kerschen, Multimodal vibration damping of nonlinear structures using multiple nonlinear absorbers, Int. J. Non-Linear Mech. 119 (2020) 103308.

[24] P. Soltani, G. Kerschen, The nonlinear piezoelectric tuned vibration absorber, Smart Mater. Struct. 24 (2015) 075015.

[25] B. Lossouarn, J.-F. Deü, G. Kerschen, A fully passive nonlinear piezoelectric vibration absorber, Phil. Trans. R. Soc. A 376 (2018) 20170142.

[26] G. Raze, A. Jadoul, S. Guichaux, V. Broun, G. Kerschen, A digital nonlinear piezoelectric tuned vibration absorber, Smart Mater. Struct. 29 (2020) 015007.

[27] C. Richard, D. Guyomar, D. Audigier, G. Ching, Semi-passive damping using continuous switching of a piezoelectric device, in: Proc. of SPIE Smart Structures and Materials Conference: Passive Damping and Isolation, Vol. 3672, 1999, pp. 104–111.

[28] W.W. Clark, Vibration control with state-switching piezoelectric material, J. Intell. Mater. Syst. Struct. 11 (2000) 263–271.

[29] P. Shivashankar, S. Gopalakrishnan, Review on the use of piezoelectric materials for active vibration, noise, and flow control, Smart Mater. Struct. 29 (2020) 053001.

[30] J. Ducarne, O. Thomas, J.-F. Deü, Structural vibration reduction by switch shunting of piezoelectric elements: modelling and optimization, J. Intell. Mater. Syst. Struct. 21 (8) (2010) 797–816, http://dx.doi.org/10.1177/1045389X10367835.

[31] O. Thomas, A. Lazarus, C. Touzé, A harmonic-based method for computing the stability of periodic oscillations of non-linear structural systems, in: Proceedings of the ASME 2010 International Design Engineering Technical Conferences & Computers and Information in Engineering Conference, IDETC/CIE 2010, Montreal, Canada, 2010.

[32] A. Givois, J.-J. Tan, C. Touzé, O. Thomas, Backbone curves of coupled cubic oscillators in one-to-one internal resonance: bifurcation scenario, measurements and parameter identification, Meccanica 55 (2020) http://dx.doi.org/10.1007/s11012-020-01132-2, 581–503.

[33] S.I. Chang, A.K. Bajaj, C.M. Krousgrill, Non-linear vibrations and chaos in harmonically excited rectangular plates with one-to-one internal resonance, Nonlinear Dynam. 4 (1993) 433–460.

[34] C. Touzé, M. Amabili, Non-linear normal modes for damped geometrically non-linear systems: application to reduced-order modeling of harmonically forced structures, J. Sound Vib. 298 (4–5) (2006) 958–981.

[35] O. Thomas, C. Touzé, Luminais, Non-linear vibrations of free-edge thin spherical shells: experiments on a 1:1:2 internal resonance, Nonlinear Dynam. 49 (1–2) (2007) 259–284, http://dx.doi.org/10.1016/j.ijsolstr.2004.10.028.

[36] A. Chaigne, C. Touzé, O. Thomas, Nonlinear vibrations and chaos in gongs and cymbals, Acoust. Sci. Technol. 26 (5) (2005) 403–409, http://dx.doi.org/10.1250/ast.26.403.

[37] M. Monteil, O. Thomas, C. Touzé, Identification of mode couplings in nonlinear vibrations of the steelpan, Appl. Acoust. 89 (2015) 1–15, http://dx.doi.org/10.1016/j.apacoust.2014.08.008.

[38] K.R. Qalandar, B.S. Strachan, B. Gibson, M. Sharma, A. Ma, S.W. Shaw, K.L. Turner, Frequency division using a micromechanical resonance cascade, Appl. Phys. Lett. 105 (2014) 244103.

[39] J. Yu, K. Asadi, H. Brahmi, H. Cho, S. Nezmi, S. Lee, Frequency stabilization in a MEMS oscillator with 1:2 internal resonance, in: 2019 IEEE International Symposium on Inertial Sensors and Systems (INERTIAL), 2019, pp. 1–4, http://dx.doi.org/10.1109/ISISS.2019.8739695.

[40] D.A. Czaplewski, S. Strachan, O. Shoshani, S.W. Shaw, D. López, Bifurcation diagram and dynamic response of a MEMS resonator with a 1:3 internal resonance, Appl. Phys. Lett. 114 (2019) 254104.

[41] G. Kerschen, M. Peeters, J.C. Golinval, A. F.Vakakis, Nonlinear normal modes, Part I : A useful framework for the structural dynamicist, Mech. Syst. Signal Process. 23 (2009) 170–194.

[42] L. Guillot, A. Lazarus, O. Thomas, C. Vergez, B. Cochelin, A purely frequency based floquet-hill formulation for the efficient stability computation of periodic solutions of ordinary differential systems, J. Comput. Phys. 416 (2020) 109477, http://dx.doi.org/10.1016/j.jcp.2020.109477.

[43] A.G. Haddow, A.D.S. Barr, D.T. Mook, Theoretical and experimental study of modal interaction in a two-degree-of-freedom structure, J. Sound Vib. 97 (3) (1984) 451–473.
[44] R.S. Haxton, A.D.S. Barr, The autoparametric vibration absorber, J. Eng. Ind. 94 (1) (1972) 119–125.
[45] A. Vyas, A.K. Bajaj, A. Raman, Dynamics of structures with wideband autoparametric vibration absorbers: theory, Proc. R. Soc. Lond. A 460 (2004) 1547–1581.
[46] S. Mahmoudkhani, H.S. Meymand, Effects of nonlinear interactions of flexural modes on the performance of a beam autoparametric vibration absorber, J. Vib. Control 26 (7–8) (2019) 459–474.
[47] S.S. Oueini, M.F. Golnaraghi, Experimental implementation of the internal resonance control strategy, J. Sound Vib. 191 (3) (1996) 377–396.
[48] S.S. Oueini, A.H. Nayfeh, M.F. Golnaraghi, A theoretical and experimental implementation of a control method based on saturation, Nonlinear Dynam. 13 (1997) 189–202.
[49] S.S. Oueini, A.H. Nayfeh, J.R. Pratt, A nonlinear vibration absorber for flexible structures, Nonlinear Dynam. 15 (1998) 259–282.
[50] P.F. Pai, B. Wen, A.S. Naser, M.J. Schultz, Structural vibration control using PZT patches and non-linear phenomena, J. Sound Vib. 215 (2) (1998) 273–296.
[51] P.F. Pai, B. Rommel, M.J. Schultz, Dynamics regulation of a skew cantilever plate using PZT patches and saturation phenomenon, J. Intell. Mater. Syst. Struct. 11 (2000) 642–655.
[52] P.F. Pai, M.J. Schultz, A refined nonlinear vibration absorber, Int. J. Mech. Sci. 42 (2000) 537–560.
[53] P.F. Pai, B. Rommel, M.J. Schultz, Non-linear vibration absorbers using higher order internal resonances, J. Sound Vib. 234 (5) (2000) 799–817.
[54] G.S. Agnes, D.J. Inman, Nonlinear piezoelectric vibration absorbers, Smart Mater. Struct. 5 (1996) 704–714.
[55] V. Guillot, A. Givois, M. Colin, O. Thomas, A.T. Savadkoohi, C.-H. Lamarque, Theoretical and experimental investigation of a 1:3 internal resonance in a beam with piezoelectric patches, J. Vib. Control 26 (13–14) (2020) 1119–1132, http://dx.doi.org/10.1177/1077546320910536.
[56] J. Kengne, J.C. Chedjou, G. Kenne, K. Kyamakya, G.H. Kom, Analog circuit implementation and synchronization of a system consisting of a van der Pol oscillator linearly coupled to a duffing oscillator, Nonlinear Dynam. 70 (2012) 2163–2173.
[57] T.M.P. Silva, M.A. Clementino, A. Erturk, C. De Marqui, Equivalent electrical circuit framework for nonlinear and high quality factor piezoelectric structures, Mechatronics 54 (2018) 133–143.
[58] O. Thomas, J.-F. Deü, J. Ducarne, Vibration of an elastic structure with shunted piezoelectric patches: efficient finite-element formulation and electromechanical coupling coefficients, Int. J. Numer. Methods Eng. 80 (2) (2009) 235–268, http://dx.doi.org/10.1002/nme.2632.
[59] M. Berardengo, O. Thomas, C. Giraud-Audine, S. Manzoni, Improved resistive shunt by means of negative capacitance: new circuit, performances and multi-mode control, Smart Mater. Struct. 25 (7) (2016) 075033, http://dx.doi.org/10.1088/0964-1726/25/7/075033.
[60] ANSI/IEEE Std 176-1987, IEEE Standard on Piezoelectricity, The Institute of Electrical and Electronics Engineers, Inc., 1988.
[61] C. Touzé, O. Thomas, A. Chaigne, Hardening/softening behaviour in non-linear oscillations of structural systems using non-linear normal modes, J. Sound Vib. 273 (1–2) (2004) 77–101, http://dx.doi.org/10.1016/j.jsv.2003.04.005.
[62] V. Denis, M. Jossic, C. Giraud-Audine, B. Chomette, A. Renault, O. Thomas, Identification of nonlinear modes using phase-locked-loop experimental continuation and normal form, Mech. Syst. Signal Process. 106 (2018) 430–452, http://dx.doi.org/10.1016/j.ymssp.2018.01.014.
[63] M. Géradin, D. Rixen, Mechanical Vibrations: Theory and Applications to Structural Dynamics, 3rd, J. Wiley & Sons, 2015.
[64] A.H. Nayfeh, D.T. Mook, Nonlinear Oscillations, John Wiley & sons, inc., New-York, 1979.
[65] O. Thomas, C. Touzé, A. Chaigne, Non-linear vibrations of free-edge thin spherical shells: modal interaction rules and 1:1:2 internal resonance, Int. J. Solids Struct. 42 (11–12) (2005) 3339–3373, http://dx.doi.org/10.1016/j.ijsolstr.2004.10.028.
[66] L. Guillot, B. Cochelin, C. Vergez, A taylor series-based continuation method for solutions of dynamical systems, Nonlinear Dynam. 98 (2019) 2827–2845.
[67] L. Guillot, B. Cochelin, C. Vergez, A generic and efficient taylor series-based continuation method using a quadratic recast of smooth nonlinear systems, Int. J. Numer. Methods Eng. 119 (2019) 261–280.
[68] B. Cochelin, M. Medale, Power series analysis as a major breakthrough to improve the efficiency of asymptotic numerical method in the vicinity of bifurcations, J. Comput. Phys. 236 (2013) 594–607.
[69] A.H. Nayfeh, R.A. Raouf, Non-linear oscillations of circular cylindrical shells, Int. J. Solids Struct. 23 (12) (1987) 1625–1638.
[70] J. Ducarne, O. Thomas, J.-F. Deü, Placement and dimension optimization of shunted piezoelectric patches for vibration reduction, J. Sound Vib. 331 (14) (2012) 3286–3303, http://dx.doi.org/10.1016/j.jsv.2012.03.002.
[71] D. Saya, D. Dezest, A.J. Welsh, F. Mathieu, O. Thomas, T. Leïchlé, S. Trolier-McKinstry, L. Nicu, Piezoelectric nanoelectromechanical systems integrating microcontact printed lead zirconate titanate films, J. Micromech. Microeng. 30 (2020) 035004, http://dx.doi.org/10.1088/1361-6439/ab60bf.
[72] A. Sénéchal, O. Thomas, J.-F. Deü, Optimization of shunted piezoelectric patches for vibration reduction of complex structures - Application to a turbojet fan blade, in: Proceedings of the ASME 2010 International Design Engineering Technical Conferences & Computers and Information in Engineering Conference, IDETC/CIE 2010, Montreal, Canada, 2010.
[73] G. Gobat, L. Guillot, A. Frangi, B. Cochelin, C. Touzé, Backbone curves, Neimark-Sacker boundaries and appearance of quasi-periodicity in nonlinear oscillators: Application to 1:2 internal resonance and frequency combs in MEMS, Meccanica 56 (8) (2021) 1937–1969.
[74] A. Renault, O. Thomas, H. Mahé, Numerical antiresonance continuation of structural systems, Mech. Syst. Signal Process. 116 (2019) 963–984, http://dx.doi.org/10.1016/j.ymssp.2018.07.005.